PHYSICS REPORTS (Review Section of Physics Letters) 199, No. 5 (1991) 231–280. North-Holland

LASER EXCITATION OF ELECTRONIC WAVE PACKETS IN RYDBERG ATOMS

G. ALBER

Fakultät für Physik, Albert-Ludwigs-Universität, Hermann-Herder-Strasse 3, D-7800 Freiburg i.Br., Fed. Rep. Germany

and

P. ZOLLER

Institut für Theoretische Physik, Universität Innsbruck, Technikerstrasse 25, A-6020 Innsbruck, Austria

Editor: J. Eichler Received March 1990

Contents:

Abstract:

We review recent theoretical and experimental work on laser-induced excitation of atomic Rydberg wave packets. Studying the motion of these wave packets provides a bridge between quantum mechanics and the classical concept of the trajectory of an electron and corresponds to real-time observations of atomic dynamics in a Coulomb, and possibly static external field. We discuss generation and detection of wave packets by short and/or intense laser pulses. On the theoretical side our emphasis is on quantum defect theory and semiclassical methods.

Single orders for this issue

PHYSICS REPORTS (Review Section of Physics Letters) 199, No. 5 (1991) 231–280.

Copies of this issue may be obtained at the price given below. All orders should be sent directly to the Publisher. Orders must be accompanied by check.

Single issue price Dfl. 37.00, postage included.

0 370-1573/91/$17.50

LASER EXCITATION OF ELECTRONIC WAVE PACKETS IN RYDBERG ATOMS

G. ALBER

Fakultät für Physik, Albert-Ludwigs-Universität, Hermann-Herder-Strasse 3, D-7800 Freiburg i.Br., Fed. Rep. Germany

and

P. ZOLLER

Institut für Theoretische Physik, Universität Innsbruck, Technikerstrasse 25, A-6020 Innsbruck, Austria

NORTH-HOLLAND

1. Introduction

The recent development of short and intense laser pulses has renewed the interest in coherent laser excitation processes of atoms and molecules [1]. Typically, in such processes a laser pulse excites a coherent superposition of atomic or molecular energy eigenstates, which represents a nonstationary charge distribution and whose subsequent time evolution is observed, for example, via the fluorescence signal or by probing the system with an external field after a variable time delay. Quantum beat spectroscopy [2] is an early example where such excitation mechanisms are used. It is based on the fact that the time dependence of the signal resulting from coherent excitation of only a few atomic or molecular energy eigenstates exhibits periodic variations or beats, whose frequencies are proportional to the corresponding energy separations. This method has been particularly successful in determining small energy differences, for example between atomic fine- or hyperfine-structure components [2].

The availability of short laser pulses in the (sub)picosecond regime [3] has opened up the possibility of exciting large numbers of atomic or molecular energy eigenstates coherently, thus preparing quantum states whose probability distribution is localized in comparison with the corresponding classically accessible region. Such wave packets are particularly interesting as they provide a bridge between quantum mechanics and the classical concept of the trajectory of a particle. Therefore, studying the evolution of these wave packets provides real-time observations of atomic or molecular dynamics.

Here, we review recent work on coherent laser excitation of Rydberg states, i.e. bound atomic or molecular energy eigenstates close to a photoionization threshold (for a review on Rydberg states see refs. [2, 4–6]). A typical property of these states is their large extension in comparison with the Bohr radius, which is the characteristic length scale for atomic and molecular quantum phenomena. This almost macroscopic size implies that, apart from a small region of a few Bohr radii around the nucleus, the dynamics of a Rydberg electron is dominantly determined by the $(1/r)$ Coulomb potential of the positively charged ionic core and that these states exhibit universal features independent of the particular atom or molecule under consideration. Effects of the ionic core can be described by a few quantum defect parameters, which take into account the scattering of the Rydberg electron inside the ionic core region [7–14].

If a superposition of many Rydberg states is excited, an electronic wave packet is generated whose time evolution reflects the motion of the excited electron in the field of the positively charged ionic core. Coherent laser excitation of Rydberg states from an energetically low lying bound state [15–37] prepares a superposition of energy eigenstates with low values of the angular momentum and the resulting electronic wave packet is only localized with respect to its radial coordinate. Because of the infinitely high level density of Rydberg states at a photoionization threshold, such *radial Rydberg wave packets* [15–27, 30–37] are always generated in laser excitation processes close to threshold and the analysis of their dynamics is therefore important for an understanding of multiphoton processes [38, 39] which involve highly excited Rydberg states as intermediate resonances. In order to localize also the angular coordinates of an electronic wave packet a superposition of states with high values of the angular momentum is needed. Starting from an energetically low lying bound state, laser excitation of such *angular wave packets* [40–45] is only possible if states with high values of the angular momentum are mixed in, for example by additional microwave [46, 47] or static fields [48]. Motivated by Schrödinger's discussion of the coherent states of the harmonic oscillator there have been various theoretical approaches to construct localized electronic wave packets which evolve along Kepler ellipses with minimum quantum fluctuations compatible with Heisenberg's uncertainty relations, thus resembling the classical motion of an electron in a Coulomb potential as closely as possible [44, 49–56].

Recently, it has been shown how, in the presence of weak, crossed static electric and magnetic fields, hydrogenic energy eigenstates which are localized along Kepler ellipses with minimum quantum fluctuations can be excited by a laser pulse [45, 48, 57]. A coherent superposition of these minimum uncertainty states with different energies would represent an ideal Kepler wave packet [45, 56].

Coherent laser excitation mechanisms have also been used to investigate chemical bond breaking and bond formation in molecules [58–74]. However, a detailed discussion of this active field of research is beyond the scope of this review. Typically, in these studies a short laser pulse with duration of a few femtoseconds prepares a molecular wave packet which is localized with respect to the internuclear separation. The internuclear distance immediately after the laser excitation process is determined by the laser frequency and the difference potential between the excited and initial state according to the Franck–Condon principle. The subsequent time evolution of this wave packet on the excited energy surface is characterized by typical dissociation times of the order of a few hundred femtoseconds and may be probed after a variable time delay with a second short laser pulse. Measuring, for example, the laser induced fluorescence from the final state as a function of the time delay between both laser pulses gives a time-resolved picture of the dynamics of the wave packet on the excited energy surface. This so-called femtosecond transition state spectroscopy [67, 68] has been applied recently to a variety of problems in connection with dissociation of molecules.

This article is organized as follows. In chapter 2 we discuss basic physical concepts which are involved in the generation and detection of Rydberg wave packets by laser-induced one-photon excitation and we review recent experimental and theoretical work. In chapter 3 we discuss in more detail theoretical methods which have been developed recently in connection with the description of the dynamics of these wave packets. In particular, we concentrate on classical path representations of atomic transition amplitudes and the minimum uncertainty states which are localized on Kepler ellipses with minimum quantum fluctuations. Finally, in chapter 4 we apply the classical path representations to the many-channel Coulomb problem and the external-field case and discuss characteristic dynamical aspects of Rydberg wave packets in these systems.

2. Rydberg wave packets: basic concepts

A typical property of an electron in a Rydberg state is its large mean distance from the nucleus in comparison with the Bohr radius [2, 4]. Depending on the angular momentum l we may distinguish two limiting cases: Rydberg states with low values of l represent electronic states which are essentially delocalized over the whole classically accessible region (corresponding to classical elliptic orbits of high eccentricity), whereas Rydberg states with extremely large angular momenta are localized essentially along a circle in a plane perpendicular to the direction of the angular momentum (corresponding to circular orbits in classical mechanics). Correspondingly, two kinds of Rydberg wave packets are discussed in the literature.

– Coherent superpositions of Rydberg states with different principal quantum number n and low values of the angular momentum l represent *radial electronic wave packets*, which are only localized with respect to the electron's distance from the nucleus. The angular coordinates are still delocalized in a quantum mechanical sense.

– In order to generate *angular electronic wave packets*, which are localized with respect to the angular coordinates, a coherent superposition of Rydberg states with high values of the angular momentum l is prepared (within one n-manifold).

The ultimate goal is to prepare a Rydberg wave packet which is localized with respect to radial and angular coordinates and moves along a Kepler ellipse with minimum quantum fluctuations compatible with Heisenberg's uncertainty relations.

Due to the infinite level density of bound states at a photoionization threshold, a radial Rydberg wave packet is always generated if Rydberg states sufficiently close to threshold are excited by a laser pulse from an energetically low lying bound state. An understanding of their dynamics is important for the interpretation of multiphoton excitation processes which involve highly excited Rydberg states as intermediate resonances. For the laser-induced excitation of angular wave packets an additional external field is needed which mixes in also states with high values of the angular momentum.

In this section we discuss basic physical concepts which are involved in laser-induced excitation of Rydberg wave packets. In section 2.1 we summarize basic properties of wave functions and dipole matrix elements of Rydberg states and the energy dependence of the atomic Green function close to a photoionization threshold. In section 2.2 we discuss generation and detection of radial Rydberg wave packets by short and intense laser pulses. Experimental and theoretical work on angular wave packets is discussed in section 2.3.

2.1. *Basic properties of Rydberg states*

Rydberg states are highly excited states in atomic systems with large principal quantum number n and, possibly, large angular momentum quantum number l [4–6]. A characteristic feature of an atom or molecule with a single excited Rydberg electron is that the electronic motion is dominated by a pure Coulomb force at large distances from the positively charged ionic core. Mathematically this may be described within the formalism of Quantum Defect Theory (QDT) [7–14], which assumes a finite-range potential of the size of the ionic core and a pure Coulomb potential for larger distances. Using the language of QDT, in this section we summarize basic properties of Rydberg states and their wave functions and discuss dipole matrix elements which describe photoabsorption to and from Rydberg states. For simplicity, we restrict our discussion to alkali atoms with one valence electron. The extension of these ideas to atoms with more than one valence electron is treated in chapters 3 and 4.

Wave functions. The wave function of an alkali atom with a single valence electron outside a closed core can be written as [9]

$$\Psi_E(R, r) = \Phi_{lm}(R) F_l(\varepsilon, r)/r\,. \tag{1}$$

The wave function of the ion core, $\Phi_{lm}(R)$, includes the angular momentum quantum numbers l and m of the valence electron. The radial wave function $F_l(\varepsilon, r)$ is a solution of the Schrödinger equation

$$\left[\varepsilon + \frac{\hbar^2}{2M_e}\left(\frac{d^2}{dr^2} - \frac{l(l+1)}{r^2}\right) - V_l(r)\right] F_l(\varepsilon, r) = 0\,, \tag{2}$$

with $E = I + \varepsilon$, the ionization energy I and the electron mass M_e. Outside the atomic core, i.e. for $r \geq r_0$, the local potential, $V_l(r)$, is well approximated by a pure $(1/r)$ Coulomb potential.

For a given energy ε, eq. (2) has two linearly independent solutions, which for $r \geq r_0$ are linear combinations of the real-valued, energy-normalized regular and irregular Coulomb functions $s_l(\varepsilon, r)$ and $c_l(\varepsilon, r)$ [12, 14]. The corresponding outgoing and incoming Coulomb waves are $\varphi_l^{\pm}(\varepsilon, r) =$

$c_l(\varepsilon, r) \pm i s_l(\varepsilon, r)$. For large values of r and $\varepsilon > 0$ the Coulomb functions $s_l(\varepsilon, r)$ and $c_l(\varepsilon, r)$ behave like sine and cosine functions of the Coulomb argument. Outside the core region the real-valued, energy-normalized regular solution, $S_l(\varepsilon, r)$, of eq. (2) is given by

$$S_l(\varepsilon, r) \sim s_l(\varepsilon, r)\cos(\pi\alpha_l) + c_l(\varepsilon, r)\sin(\pi\alpha_l)\,. \tag{3}$$

The quantum defect, α_l, describes the deviation of the potential $V_l(r)$ from a pure $(1/r)$ Coulomb potential inside the core region. The corresponding irregular solution of eq. (2), $C_l(\varepsilon, r)$, behaves asymptotically like

$$C_l(\varepsilon, r) \sim -s_l(\varepsilon, r)\sin(\pi\alpha_l) + c_l(\varepsilon, r)\cos(\pi\alpha_l)\,. \tag{4}$$

Semiclassically, the regular radial wave function of eq. (3) is [75]

$$S_l(\varepsilon, r) \sim (\mathcal{R}y\, a_0 \pi)^{-1/2}[p(r)a_0/\hbar]^{-1/2} \sin\left(\int_{r_1}^{r} \mathrm{d}r'\; p(r')/\hbar - (l+1/2)\pi + \pi/4\right) \quad (r_1 \ll r \ll r_2)\,, \tag{5}$$

with the Rydberg energy $\mathcal{R}y = M_e e^4/(2\hbar^2) \approx 13.6\,\mathrm{eV}$ and the Bohr radius $a_0 = \hbar^2/(M_e e^2) \approx 5.29 \times 10^{-11}$ m. The radial momentum of zero angular momentum, $p(r)$, is given by

$$p(r) = \{2M_e[E - V_l(r)]\}^{1/2}\,, \tag{6}$$

with $p(r_1) = p(r_2) = 0$ at the classical turning points r_1 and r_2.

The radial wave functions considered in the context of scattering theory and photoionization will be denoted by $\mathcal{F}_l^{(+)}(\varepsilon, r)$ and $\mathcal{F}_l^{(-)}(\varepsilon, r)$, respectively. They are defined as energy-normalized regular solutions of eq. (2) with an incoming (outgoing) Coulomb wave and a phase-shifted outgoing (incoming) Coulomb wave,

$$\mathcal{F}_l^{(\pm)}(\varepsilon, r) = (\mp i)\, e^{\pm i\pi\alpha_l} S_l(\varepsilon, r) \sim \tfrac{1}{2}[\varphi_l^{\mp}(\varepsilon, r) - e^{\pm 2i\pi\alpha_l}\varphi_l^{\pm}(\varepsilon, r)]\,. \tag{7}$$

Below threshold, i.e. for $\varepsilon < 0$, $\varphi_l^{\pm}(\varepsilon, r)$ can be decomposed into exponentially growing and decaying functions $J_l(\varepsilon, r)$ and $P_l(\varepsilon, r)$ [9, 12] according to

$$\varphi_l^{\pm}(\varepsilon, r) = e^{\pm i\pi\nu}[J_l(\varepsilon, r) \mp i(\mathrm{d}\varepsilon/\mathrm{d}\nu)^{-1/2} P_l(\varepsilon, r)] \quad (\varepsilon < 0)\,. \tag{8}$$

Here, $P_l(\varepsilon, r)$ is normalized to one. The conversion factor $\mathrm{d}\varepsilon/\mathrm{d}\nu = 2\mathcal{R}y/\nu^3$ is the energy density of the Rydberg states as derived from the relation $\varepsilon = -\mathcal{R}y/\nu^2$ with the effective quantum number ν. The requirement that the wave function of a bound state should be normalizable implies that the coefficient of the exponentially growing part must be zero. This gives rise to the quantization condition

$$\varepsilon_{nl} = -\mathcal{R}y/\nu_{nl}^2\,, \tag{9}$$

with $\nu_{nl} = n - \alpha_l$ and $n = l+1, l+2, \ldots$. The corresponding bound state eigenfunctions are

$$P_{nl}(r) = (\mathrm{d}\varepsilon_{nl}/\mathrm{d}n)^{1/2} S_l(\varepsilon_{nl}, r)\,. \tag{10}$$

Dipole matrix elements. We define dipole matrix elements for photoionization from an energetically low lying atomic state $|\mathrm{i}\rangle$ to a continuum state $|\varepsilon lm\rangle$ by

$$\mathscr{D}^{(-)}_{\varepsilon lm,\mathrm{i}} = \int_0^\infty \mathrm{d}r\, r[\mathscr{F}^{(-)}_l(\varepsilon, r)]^* \langle \Phi_{lm} | \boldsymbol{\mu}\cdot\boldsymbol{\varepsilon} | \mathrm{i}\rangle_r , \tag{11}$$

with the dipole operator $\boldsymbol{\mu}$ and the light polarization vector $\boldsymbol{\varepsilon}$ [9]. In a similar way transition matrix elements to Rydberg states are defined by

$$\mathscr{D}_{nlm,\mathrm{i}} = \langle nlm | \boldsymbol{\mu}\cdot\boldsymbol{\varepsilon} | \mathrm{i}\rangle = \mathrm{i}(\mathrm{d}\varepsilon_{nl}/\mathrm{d}n)^{1/2}\, \mathrm{e}^{-\mathrm{i}\pi\alpha_l} \mathscr{D}^{(-)}_{\varepsilon lm,\mathrm{i}} . \tag{12}$$

The dipole matrix elements of eq. (11) are smooth functions of energy across threshold. This is due to the finite size of the energetically low lying state $|\mathrm{i}\rangle$, which implies that the contributions to the dipole matrix element come from distances much smaller than the typical extension of a Rydberg state. In a similar way, matrix elements for free–free transitions are defined by

$$\mathscr{D}^{(-+)}_{\varepsilon' l'm',\varepsilon lm} = \int_0^\infty \mathrm{d}r\, [\mathscr{F}^{(-)}_{l'}(\varepsilon', r)]^* \langle \Phi_{l'm'} | \boldsymbol{\mu}\cdot\boldsymbol{\varepsilon} | \Phi_{lm}\rangle_r \mathscr{F}^{(+)}_l(\varepsilon, r) , \tag{13}$$

and are related to Rydberg–free dipole matrix elements by

$$\mathscr{D}^{(-)}_{\varepsilon' l'm',nlm} = \mathrm{i}(\mathrm{d}\varepsilon_{nl}/\mathrm{d}n)^{1/2}\, \mathrm{e}^{-\mathrm{i}\pi\alpha_l} \mathscr{D}^{(-+)}_{\varepsilon' l'm',\varepsilon lm} . \tag{14}$$

For a fixed value of the energy difference, $\varepsilon' - \varepsilon = \hbar\omega$, these free–free matrix elements are slowly varying functions of energy across threshold as long as energy variations are smaller than the transition energy $\hbar\omega$. This property becomes apparent when the dipole matrix element of eq. (13) is converted from length form to acceleration form. Then the corresponding radial integral becomes proportional to [76, 77]

$$\lim_{r\to\infty} \int_0^r \mathrm{d}r'\, S_{l'}(\varepsilon', r') \frac{\mathrm{d}V_l(r')}{\mathrm{d}r'} S_l(\varepsilon, r') , \tag{15}$$

and the contribution is built up from an interaction volume which is *much smaller than the size of Rydberg states*, as may be seen from fig. 1. Physically speaking, this is due to the fact that the electron can only absorb the photon near the inner turning point of its orbit. Far away from the nucleus the electron behaves like a free particle and does not absorb radiation. This property will become important below in our study of absorption and emission of optical photons, because it means that a wave packet can only absorb or emit radiation near the inner turning point of a Kepler orbit. A general discussion of the finite range of the radiative interaction in optical transitions has been given in refs. [78, 79].

Green function. In the following section we will need the retarded Green function of the atomic Schrödinger equation,

$$G^+(E) = \frac{1}{E - H_\mathrm{A} + \mathrm{i}0} \equiv \sum_{nlm} \int \frac{|nlm\rangle\langle nlm|}{E - E_{nl} + \mathrm{i}0} , \tag{16}$$

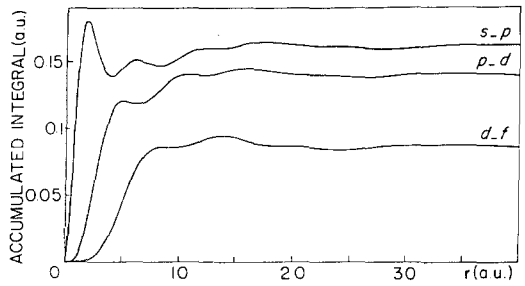

Fig. 1. Convergence of the radial dipole integral form for $(l \to l+1)$ transitions as a function of the upper integration limit, r, for $\varepsilon = 0$, $\varepsilon' = 0.3\mathcal{R}y$ and $(l, l') = (0,1), (1,2), (2,3)$. The finite range of the radiative interaction is illustrated by the convergence of the radial integral with r. For higher l-values the radial integrals are built at larger distances and decrease in magnitude due to the increasing centrifugal barrier [78].

with the atomic Hamiltonian H_A and its energy eigenvalues $E_{nl} = I + \varepsilon_{nl}$. Analogous to eq. (1), one can factorize $G^+(E)$ into a core or angular part and a radial Green function. For energies $\varepsilon > 0$, the radial Green function is given by

$$g_l^{s+}(\varepsilon; r, r') = -\pi S_l(\varepsilon, r_<)\varphi_l^+(\varepsilon, r_>)\,, \tag{17}$$

with $r_>$ and $r_<$ the larger and smaller of r and r'. Below threshold, i.e. for $\varepsilon < 0$, eq. (17) diverges for $r \to \infty$ and no longer represents the radial part of eq. (16). For these energies the *physical Green function* can be constructed by adding to $g_l^{s+}(\varepsilon; r, r')$ a multiple of the regular solution of the radial Schrödinger equation (2) in order to enforce the correct asymptotic behavior. Using well-known properties of Coulomb functions [9] we obtain

$$g_l^+(\varepsilon; r, r') = g_l^{s+}(\varepsilon; r, r') + 2\pi i \frac{\mathcal{F}_l^{(+)}(\varepsilon, r)[\mathcal{F}_l^{(-)}(\varepsilon, r')]^*}{e^{-2\pi i\nu} - e^{2\pi i\alpha_l}} \quad (\varepsilon < 0, \operatorname{Im}\varepsilon > 0)\,. \tag{18}$$

This radial Green function has poles at the bound-state energies $\varepsilon_{nl} = -\mathcal{R}y/(n-\alpha_l)^2$.

Expanding the resonant denominator in eq. (18) into a geometric series we find

$$g_l^+(\varepsilon; r, r') = g_l^{s+}(\varepsilon; r, r') + 2\pi i \mathcal{F}_l^{(+)}(\varepsilon, r)\, e^{2i\pi\nu} \sum_{M=0}^{\infty} (e^{2i\pi\alpha}\, e^{2i\pi\nu})^M [\mathcal{F}_l^{(-)}(\varepsilon, r')]^* \quad (\operatorname{Im}\varepsilon > 0)\,. \tag{19}$$

Equation (19) is a *classical path representation*, which will be discussed in a more general context in chapter 3. Briefly speaking, the contributions from $M = 0, 1, 2, \ldots$ may be attributed to the first, second, etc. revolution of the excited electron along its orbit.

2.2. Radial Rydberg wave packets

In this section we discuss basic physical concepts which are involved in the generation and detection of Rydberg wave packets by short and intense laser pulses. In particular, we consider a laser-induced one-photon excitation process as schematically shown in fig. 2. An atomic electron is excited from an energetically low lying atomic state $|i\rangle$ with energy E_i to Rydberg states by absorption of a single laser photon. At the position of the atom, $x = 0$, the laser pulse may be described by the classical electric

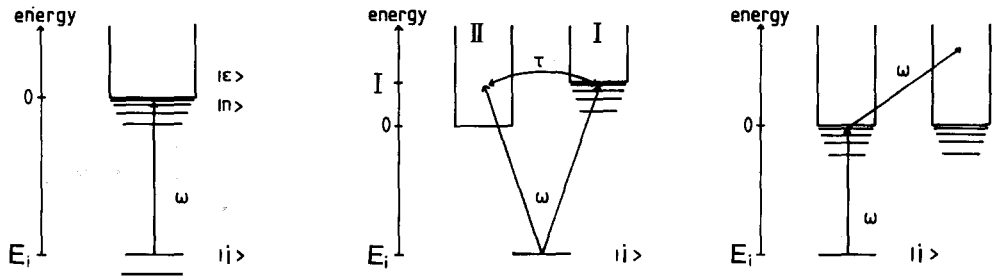

Fig. 2. Schematic representation of excitation processes studied in chapter 2.

field

$$\boldsymbol{E}(\boldsymbol{x}=0,t)=\mathscr{E}_a(t)\boldsymbol{\varepsilon}_a\,e^{-i\omega_a t}+\text{c.c.}\,, \tag{20}$$

with the laser frequency ω_a, the polarization vector $\boldsymbol{\varepsilon}_a$ and the slowly varying complex amplitude $\mathscr{E}_a(t)$.

For the wave function of the atom we make the ansatz

$$|\Psi(t)\rangle=|i\rangle a_i(t)+\sum_{nlm}\int a_{nlm}(t)|nlm\rangle=|i\rangle a_i(t)+|F(t)\rangle\,. \tag{21}$$

Here, $|F(t)\rangle$ characterizes the time evolution of the excited Rydberg electron and $a_{nlm}(t)$ are the corresponding Rydberg amplitudes. From the time-dependent Schrödinger equation we find in the rotating-wave approximation

$$\begin{aligned}
i\hbar\frac{d}{dt}a_i(t)&=E_i a_i(t)-\sum_{nlm}\int\langle i|\boldsymbol{\mu}\cdot\boldsymbol{\varepsilon}_a^*|nlm\rangle\,\mathscr{E}_a(t)^*\,e^{i\omega_a t}a_{nlm}(t)\,,\\
i\hbar\frac{d}{dt}a_{nlm}(t)&=E_{nlm}a_{nlm}(t)-\langle nlm|\boldsymbol{\mu}\cdot\boldsymbol{\varepsilon}_a|i\rangle\,\mathscr{E}_a(t)\,e^{-i\omega_a t}a_i(t)\,.
\end{aligned} \tag{22}$$

In subsections 2.2.1 and 2.2.3 we will solve this equation with the help of methods which are derived from QDT [17, 18, 30, 32]. This approach has the advantage of providing a clear physical interpretation of the formation of Rydberg wave packets and it is closely related to semiclassical methods of quantum mechanics. This aspect will be discussed in more detail in connection with classical path representations of atomic transition amplitudes in chapter 3. Numerical solutions of this equation have been obtained by Stroud and coworkers in modeling their wave packet experiments [15, 40, 41]. Wave packet solutions of eq. (22) were also discussed by Fedorov et al. [28, 31, 35] and Grochmalicki and Lewenstein [33].

2.2.1. Generation by a short laser pulse

In this subsection we solve eq. (22) for the case of a weak and short laser pulse which still contains many optical oscillations. Thus, we assume that all laser-induced time scales, for example the depletion time of the initial state, are much longer than the pulse duration. In this limit eq. (22) may be solved perturbatively with respect to the laser field and we find

$$|F(t)\rangle=\frac{i}{\hbar}\sum_{nlm}|nlm\rangle\,e^{-iE_{nl}t/\hbar}\int_{-\infty}^{t}dt'\,\langle nlm|\boldsymbol{\mu}\cdot\boldsymbol{\varepsilon}_a|i\rangle\,\mathscr{E}_a(t')\,e^{i(E_{nl}-E_i-\hbar\omega_a)t'/\hbar}\,. \tag{23}$$

Long after the interaction with the laser pulse, the Rydberg amplitudes are given by

$$a_{nlm}(t) = (\mathrm{i}/\hbar)\langle nlm|\boldsymbol{\mu}\cdot\boldsymbol{\varepsilon}_\mathrm{a}|\mathrm{i}\rangle\,\tilde{\mathscr{E}}_\mathrm{a}(\delta^\mathrm{a}_{E_{nl}})\exp(\mathrm{i}\delta^\mathrm{a}_{E_{nl}}t_\mathrm{a})\,\mathrm{e}^{-\mathrm{i}E_{nl}t/\hbar}\,, \tag{24}$$

with the detuning $\delta^\mathrm{a}_{E_{nl}} = (E_{nl} - E_\mathrm{i} - \hbar\omega_\mathrm{a})/\hbar$. The laser pulse is centered around time t_a with pulse duration τ_a and $\tilde{\mathscr{E}}_\mathrm{a}(\Delta) = \int_{-\infty}^{\infty}\mathrm{d}t\,\mathscr{E}(t+t_\mathrm{a})\,\mathrm{e}^{\mathrm{i}\Delta t}$ is its Fourier transform. Hence, laser excitation by a pulse with pulse duration τ_a leads to significant excitation of Rydberg states with energies $E_\mathrm{i} + \hbar\omega_\mathrm{a} - \hbar/\tau_\mathrm{a} \le E \le E_\mathrm{i} + \hbar\omega_\mathrm{a} + \hbar/\tau_\mathrm{a}$.

If the exciting laser pulse is short in the sense that its spectral width overlaps many Rydberg states, i.e.,

$$\frac{\hbar}{\tau_\mathrm{a}} \gg \frac{1}{2\pi}\left.\frac{\mathrm{d}E_{nl}}{\mathrm{d}n}\right|_{\bar{n}}\,, \tag{25}$$

with the mean excited energy $E_{\bar{n}} = E_\mathrm{i} + \hbar\omega_\mathrm{a}$, many terms contribute to the sum of eq. (23) and $|F(t)\rangle$ describes an electronic wave packet. As the classical orbit time of an electron with mean excited energy $E_{\bar{n}}$ is given by

$$T_{E_{\bar{n}}} = 2\pi\,\frac{\hbar}{2\mathscr{R}y}\left(-\frac{E_{\bar{n}}}{\mathscr{R}y}\right)^{-3/2} = 2\pi\nu^3_{\bar{n}}t_\mathrm{au}\,, \tag{26}$$

eq. (25) states that a wave packet is excited whenever the pulse duration is shorter than the classical orbit time of the excited electron ($t_\mathrm{au} \approx 2.42\times 10^{-17}$ s is the atomic time unit). Dipole selection rules imply that only a few angular momentum eigenstates contribute to the sum in eq. (23). Therefore, only the radial coordinate of this wave packet is localized. The angular coordinates are still delocalized in a quantum mechanical sense. The essential element in eq. (23) responsible for the wave packet structure is the coherence in the superposition of many Rydberg states.

For a discussion of the time evolution of this wave packet it is convenient to replace the sum over n in eq. (23) by an integral. This can be achieved by rewriting eq. (23) with the help of the resolvent of eq. (16),

$$|F(t)\rangle = -\frac{1}{2\pi\hbar}\int_{-\infty}^{\infty}\mathrm{d}E\,\mathrm{e}^{-\mathrm{i}Et/\hbar}G^+(E)\boldsymbol{\mu}\cdot\boldsymbol{\varepsilon}_\mathrm{a}|\mathrm{i}\rangle\,\tilde{\mathscr{E}}_\mathrm{a}(\delta^\mathrm{a}_E)\exp(\mathrm{i}\delta^\mathrm{a}_E t_\mathrm{a})\,. \tag{27}$$

Inserting the classical path representation of eq. (19) we find for $r > r_0$

$$\begin{aligned} F(R,r,t) = -\frac{\mathrm{i}}{\hbar}\sum_{lm}\Phi_{lm}(R)\,\frac{1}{r}\int_{-\infty}^{\infty}\mathrm{d}E\,\mathrm{e}^{-\mathrm{i}Et/\hbar}\tilde{\mathscr{E}}_\mathrm{a}(\delta^\mathrm{a}_E)\exp(\mathrm{i}\delta^\mathrm{a}_E t_\mathrm{a}) \\ \times\Bigg(\frac{1}{2\pi\mathrm{i}}\int_0^\infty\mathrm{d}r'\,r' g^{s+}_l(\varepsilon;r,r')\langle\Phi_{ml}|\boldsymbol{\mu}\cdot\boldsymbol{\varepsilon}_\mathrm{a}|\mathrm{i}\rangle_{r'} \\ +\sum_{M=0}^{\infty}\mathrm{e}^{2\pi\mathrm{i}\nu}(\mathrm{e}^{2\pi\mathrm{i}\alpha_l}\,\mathrm{e}^{2\pi\mathrm{i}\nu})^M\mathscr{F}^{(+)}_l(\varepsilon,r)\mathscr{D}^{(-)}_{\varepsilon lm,\mathrm{i}}\Theta(-\varepsilon)\Bigg)\quad (E = I+\varepsilon)\,. \end{aligned} \tag{28}$$

An equivalent result can be obtained directly from eq. (23) with the help of the Poisson summation formula. If many states contribute to eq. (23) the energy integrals of eq. (28) can be evaluated in a stationary phase approximation. This leads to the following interpretation of the various terms.

(i) *Wave packet in the continuum.* If the laser pulse excites dominantly continuum states, only the first term in eq. (28) contributes and the radial center of the wave packet, $r(t)$, escapes to infinity.

(ii) *Bound wave packet.* If the laser pulse excites a superposition of Rydberg states, for small times, $t - t_a < T_{E_{\bar{n}}}/2$, only the first term of eq. (28) contributes significantly. We emphasize that – although we have a bound particle – its motion is governed by the continuum propagator $g_l^{s+}(\varepsilon; r, r')$. This is not surprising, because for these times the electron has not yet been reflected at the outer turning point of its orbit. At time $t - t_a \approx T_{E_{\bar{n}}}/2$ the wave packet returns again to the ionic core region. The periodic motion of the electron is described by the infinite sum in eq. (28). From the stationary phase condition

$$\pm \int_{r_1}^{r(t)} \frac{M_e}{p(r')}\, dr' = t - t_a - (M+1)T_{E_{\bar{n}}} \quad (M = 0, 1, \ldots), \tag{29}$$

we realize that the Mth term in the sum is the contribution from the $(M+1)$th return of the excited electron, which moves along the bound Kepler orbit.

Figures 3a,b show the motion of a radial packet when a laser pulse with $\tau_a = 8$ ps excites hydrogenic Rydberg states with $l = 1$ around $\bar{n} = 85$. This corresponds to a mean classical orbit time of $T = 94$ ps. The generated wave packet is plotted for times $t - t_a = \frac{1}{9}T, \frac{2}{9}T, \frac{3}{9}T$. Figure 3b compares the wave

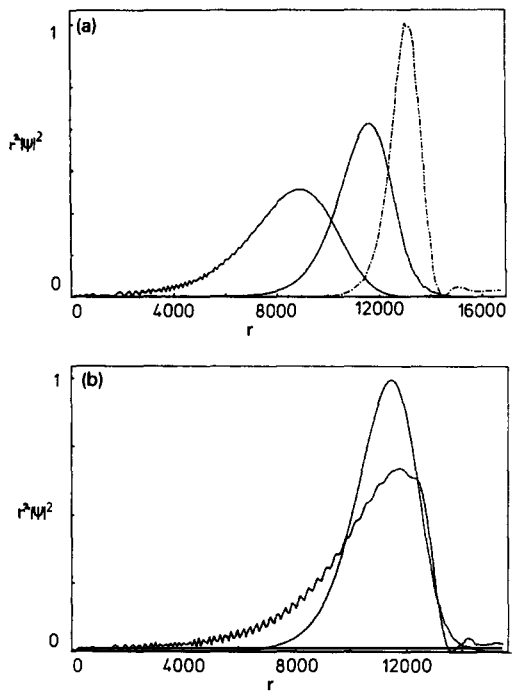

Fig. 3. Radial Rydberg wave packet in hydrogen as a function of r (in units of the Bohr radius a_0). A laser pulse of duration 8 ps induces an (s→p) transition around $\bar{n} = 85$ corresponding to $T = 94$ ps (from ref. [17]). (a) Probability $|r\Psi(r, t)|^2$ at $t - t_a = (1/9)T$, $(2/9)T$, $(3/9)T$. (b) Probability $|r\Psi(r, t)|^2$ at $t - t_a = (2/9)T$ and $(1 + 2/9)T$.

packet at times $t - t_a = \frac{2}{9}T$ and $t - t_a = (1 + \frac{2}{9})T$. As is apparent from fig. 3b, the wave packet tends to spread with time. Figure 4 is a three-dimensional plot of the probability density of the Rydberg wave packet. The angular part is a p-wave.

The uncertainty product of the wave packet during its evolution has been studied in ref. [15]. Its initial width is found to be close to the minimum uncertainty limit, but spreads rapidly as the wave packet evolves.

Revivals. The anharmonicity of the level spacing leads to a destruction of the coherence of the wave packet in the course of many classical orbiting periods T_{cl}. This restricts the duration of the "classical" evolution where the wave packet is well defined. For long times the dephasing need not be completely irreversible and there is the possibility for the wave packet to regain its initial shape (revival of the wave packet). This aspect was studied numerically in ref. [15]. As an example, fig. 5 shows the emission spectrum of an atom excited by a short laser pulse (10 ps) around $\bar{n} = 85$ with $T_{cl} = 94$ ps as calculated by Parker and Stroud [15]. A complete reconstruction of the wave packet is observed after approximately 35 periods of classical motion. There are also other (fractional) revivals, which are indicated by arrows. An analytical discussion of these fractional revivals was given by Averbukh and Perelman [23]. Keeping only second-order terms in the anharmonicity of the atomic levels, the excited state is given by

$$|F(t)\rangle = \sum_n a_n(t)|n\rangle \exp[-2\pi i(\Delta n\, t/T_{cl} + \Delta n^2\, t/T_{rev})]\,, \tag{30}$$

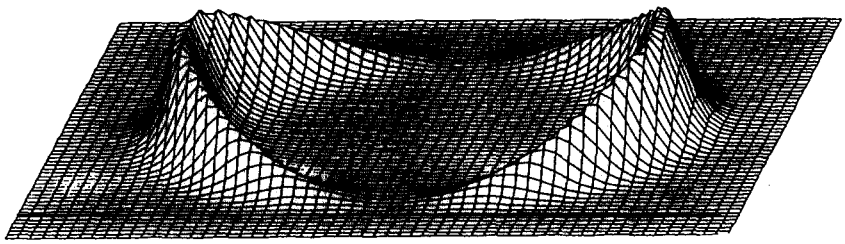

Fig. 4. Projection of the probability density $|r\Psi(r, t)|^2$ of a radial Rydberg wave packet ($l = 1$, $m = 0$) onto the y–z plane is shown at $t = (1/2)T$ (parameters as in fig. 3).

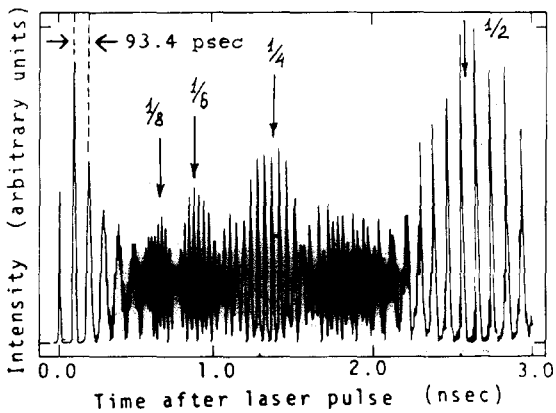

Fig. 5. The emission of an atom excited by a short laser pulse to highly excited Rydberg states (according to ref. [15]). Fractional revivals are indicated by arrows [23].

with $\Delta n = n - \bar{n}$ and $T_{\rm rev}$ the revival time. One can define a "classical" wave packet evolving without dispersion by

$$|F(t)\rangle_{\rm cl} = \sum_n a_n(t)|n\rangle \exp(-2\pi {\rm i}\,\Delta n\, t/T_{\rm cl})\,, \tag{31}$$

so that $|F(t)\rangle \sim |F(t)\rangle_{\rm cl}$ for $t \ll T_{\rm rev}$. For $t \approx T_{\rm rev}$ the additional phase shift due to the anharmonicity drops out and we have a revival, because $|F(t)\rangle \sim |F(t)\rangle_{\rm cl}$. In ref. [23] the scenario of fractional revivals is discussed. The simplest occurs at $t \sim \frac{1}{2}T_{\rm rev}$, where $|F(t)\rangle \sim |F(t+\frac{1}{2}T_{\rm cl})\rangle_{\rm cl}$. Another one takes place at $t \sim \frac{1}{4}T_{\rm rev}$, where

$$|F(t)\rangle \sim (1/\sqrt{2})[{\rm e}^{-{\rm i}\pi/4}|F(t)\rangle_{\rm cl} + {\rm e}^{+{\rm i}\pi/4}|F(t+\tfrac{1}{2}T_{\rm cl})\rangle_{\rm cl}]\,. \tag{32}$$

Equation (32) represents a nonclassical object formed by two correlated wave packets which are spatially separated within the classical orbit. The arrows in fig. 5 indicate the times $\frac{1}{8}T_{\rm rev}$, $\frac{1}{6}T_{\rm rev}$, $\frac{1}{4}T_{\rm rev}$ and $\frac{1}{2}T_{\rm rev}$, which correspond to these fractional revivals.

Two-photon excitation and quadratic Stark shift. The experiments discussed in subsection 2.2.2 use two-photon excitation schemes for creating Rydberg wave packets. It is straightforward to generalize eq. (22) to two-photon absorption. If the intermediate states are nonresonant, they can be eliminated in perturbation theory. This leads again to equations of the form (22) where the one-photon dipole matrix element is replaced by an effective two-photon matrix element,

$$\langle nlm|\boldsymbol{\mu}\cdot\boldsymbol{\varepsilon}|{\rm i}\rangle\,\mathscr{E}(t) \to \sum_r \int \frac{\langle nlm|\boldsymbol{\mu}\cdot\boldsymbol{\varepsilon}|r\rangle\langle r|\boldsymbol{\mu}\cdot\boldsymbol{\varepsilon}|{\rm i}\rangle}{E_{\rm i}+\hbar\omega-E_r}\,\mathscr{E}(t)^2\,. \tag{33}$$

In the same order of perturbation theory the initial state and the Rydberg states are Stark shifted by the amount

$$\delta E_k = \sum_r \int \left(\frac{|\langle r|\boldsymbol{\mu}\cdot\boldsymbol{\varepsilon}|k\rangle|^2}{E_k+\hbar\omega-E_r} + \frac{|\langle r|\boldsymbol{\mu}\cdot\boldsymbol{\varepsilon}^*|k\rangle|^2}{E_k-\hbar\omega-E_r}\right)|\mathscr{E}(t)|^2\,, \tag{34}$$

with $k = {\rm i}$ or $k = (nlm)$. Close to threshold, i.e. for frequencies $\hbar\omega \gg |\varepsilon_{nl}|$, the Stark shift of the Rydberg states is approximately given by

$$\delta E_{nlm} = \frac{e^2}{M_e\omega^2}\,|\mathscr{E}(t)|^2 + {\rm O}(\nu_{nl}^{-3})\,, \tag{35}$$

and is only weakly dependent on n [78]. The first term in this equation is just the shift of the ionization threshold due to the wiggle energy of the electron in the laser field. This ponderomotive shift of the Rydberg threshold has been discussed at length in recent literature on the electron spectrum in above-threshold ionization (for references see refs. [80, 39]). In our context, the intensity dependence of the Stark shift leads to a time-dependent phase in eq. (23), similar to a frequency chirp of the laser pulse. A detailed numerical study of the effect of the Stark shift in potassium is given in refs. [24, 25]. In this case the shift of the ground state is the dominant factor. These authors come to the conclusion that the Stark effect places an upper limit on the strength of the pulse that can be used to excite a

"good" radial wave packet. Noordam et al. [26] considered a situation where the shift of the Rydberg states dominates. In this case the Stark shift leads to a contraction of the wave packet with the first return to the core. A similar effect has been found in ref. [17] in the case of a frequency chirp of the laser pulse. Noordam et al. suggest to use excited Rydberg systems as an amplifying laser medium and to exploit this effect to shorten laser pulses efficiently.

2.2.2. Detection of a Rydberg wave packet

According to Parker and Stroud [15] the motion of an electronic wave packet can be observed by monitoring the time dependence of the light emitted by the orbiting atomic electron. The returns of the electron to the ion core manifest themselves as spikes of the intensity, which repeat themselves with the classical orbit time until the wave packet decays.

Here, we discuss in some detail the concept of observing the wave packet dynamics in two-photon processes with time delayed pump and probe pulses as suggested by Alber et al. and Henle et al. [17, 18]. Similar configurations have been studied by Fedorov and coworkers [31, 35]. Two recent experiments have employed this technique [21, 25].

We assume a first pump pulse $\mathscr{E}_a(t)$ to excite a wave packet at time t_a, which is probed at a later time $t_b > t_a + \tau_a$ by a second short pulse $\mathscr{E}_b(t)$ of duration τ_b and mean frequency ω_b. The conceptually simplest version of such a two-photon detection scheme is a two-color Raman-type process where the second pulse de-excites the electron by stimulated emission to a (low lying) bound state $|f\rangle$ with energy E_f. Using perturbation theory, the probability of finding the electron in state $|f\rangle$ is given by

$$P_{fi} = \left| \frac{i}{\hbar} \int_{-\infty}^{t} dt' \, e^{-iE_f(t-t')/\hbar} \langle f | \boldsymbol{\mu} \cdot \boldsymbol{\varepsilon}_b^* | F(t') \rangle \, \mathscr{E}_b^*(t') \, e^{i\omega_b t'} \right|^2 . \tag{36}$$

As is apparent from eq. (36), the wave packet $|F(t)\rangle$ can only be de-excited when there is significant overlap with the (localized) final state $|f\rangle$. Hence, we expect P_{fi} to show maxima when t_b coincides with the return of the wave packet to the inner turning point of its orbit. According to eq. (27), long after the interaction with the second laser pulse the transition probability is given by

$$P_{fi} = \left| \frac{1}{2\pi\hbar^2} \int_{-\infty}^{\infty} dE \, \tilde{\mathscr{E}}_b^*(\delta_E^b) \tilde{\mathscr{E}}_a(\delta_E^a) T_{fi}(E) \exp(-i\delta_E^b t_b + i\delta_E^a t_a) \right|^2 \tag{37}$$

with the two-photon transition matrix element

$$\begin{aligned} T_{fi}(E) &= \langle f | \boldsymbol{\mu} \cdot \boldsymbol{\varepsilon}_b^* G^+(E + i0) \boldsymbol{\mu} \cdot \boldsymbol{\varepsilon}_a | i \rangle \\ &\equiv \sum_{nlm} \int \langle f | \boldsymbol{\mu} \cdot \boldsymbol{\varepsilon}_b^* \frac{|nlm\rangle\langle nlm|}{E - E_{nl} + i0} \boldsymbol{\mu} \cdot \boldsymbol{\varepsilon}_a | i \rangle , \end{aligned} \tag{38}$$

and the detunings $\delta_E^a = (E - \hbar\omega_a - E_i)/\hbar$, $\delta_E^b = (E - \hbar\omega_b - E_f)/\hbar$. Equation (18) implies a two-photon matrix element of the form

$$T_{fi}(E) = \begin{cases} T_{fi}^s(E) & (\varepsilon > 0) , \\ T_{fi}^s(E) + 2\pi i \, \Sigma_{lm} \, \mathscr{D}_{f,\varepsilon lm}^{(+)} (e^{-2\pi i\nu} - e^{2\pi i\alpha_l})^{-1} \mathscr{D}_{\varepsilon lm,i}^{(-)} & (\varepsilon < 0, \operatorname{Im}\varepsilon > 0) , \end{cases} \tag{39}$$

with $E = I + \varepsilon$. Thus, for $\varepsilon < 0$ the two-photon matrix element consists of two parts: The first part is the two-photon matrix element, $T_{\mathrm{fi}}^{\mathrm{s}}(E)$, which is smoothly extrapolated from the energy region above threshold. The second term has singularities whenever E coincides with one of the Rydberg energies. $\mathscr{D}_{\mathrm{f},\varepsilon lm}^{(+)}$ and $\mathscr{D}_{\varepsilon lm,\mathrm{i}}^{(-)}$ are dipole matrix elements which are smoothly extrapolated to below threshold. Figure 6 illustrates the energy dependence of the two-photon transition amplitude of eq. (39) for hydrogen [79]. In eq. (39) the rapid energy dependence associated with Rydberg resonances has been separated from the quantities $T_{\mathrm{fi}}^{\mathrm{s}}(E)$, $\mathscr{D}_{\mathrm{f},\varepsilon lm}^{(+)}$, $\mathscr{D}_{\varepsilon lm,\mathrm{i}}^{(-)}$ and α_l, which are slowly varying functions of energy across the Rydberg threshold and can be taken as constants for our purposes. This separation is vital for evaluating the energy integrals of eq. (37). From a physical point of view, the existence of these slowly varying functions of energy reflects the fact that, apart from the pure Coulomb force, the interaction of the Rydberg electron with the radiation field and the ion core is confined to a finite interaction volume which is much smaller than the size of the Rydberg states.

From eq. (19) we obtain the classical path representation of the two-photon transition probability,

$$P_{\mathrm{fi}} = \left| \frac{1}{\hbar^2} \left(\frac{1}{2\pi \mathrm{i}} \int_{-\infty}^{\infty} \mathrm{d}E\, \tilde{\mathscr{E}}_{\mathrm{b}}^{*}(\delta_E^{\mathrm{b}}) \tilde{\mathscr{E}}_{\mathrm{a}}(\delta_E^{\mathrm{a}}) T_{\mathrm{fi}}^{\mathrm{s}}(E) \exp(\mathrm{i}\delta_E^{\mathrm{a}} t_{\mathrm{a}} - \mathrm{i}\delta_E^{\mathrm{b}} t_{\mathrm{b}}) \right.\right.$$

$$\left.\left. + \sum_{lm} \int_{-\infty}^{I} \mathrm{d}E\, \mathscr{D}_{\mathrm{f},\varepsilon lm}^{(+)} \tilde{\mathscr{E}}_{\mathrm{b}}^{*}(\delta_E^{\mathrm{b}})\, \mathrm{e}^{2\pi \mathrm{i}\nu} \sum_{M=0}^{\infty} (\mathrm{e}^{2\mathrm{i}\pi\alpha_l}\, \mathrm{e}^{2\mathrm{i}\pi\nu})^M \mathscr{D}_{\varepsilon lm,\mathrm{i}}^{(-)} \tilde{\mathscr{E}}_{\mathrm{a}}(\delta_E^{\mathrm{a}}) \exp(\mathrm{i}\delta_E^{\mathrm{a}} t_{\mathrm{a}} - \mathrm{i}\delta_E^{\mathrm{b}} t_{\mathrm{b}}) \right) \right|^2 . \quad (40)$$

Following the discussion of the previous section, the various terms in eq. (40) can be interpreted as follows.

(i) If the pump laser is tuned to the continuum, there is only a contribution from the first term of eq. (40), which involves the continuum propagator $g_l^{\mathrm{s}+}(\varepsilon; r, r')$. Therefore, P_{fi} will be essentially nonzero only for overlapping laser pulses with $t_{\mathrm{b}} \approx t_{\mathrm{a}}$. The physical picture behind this is that the pump pulse

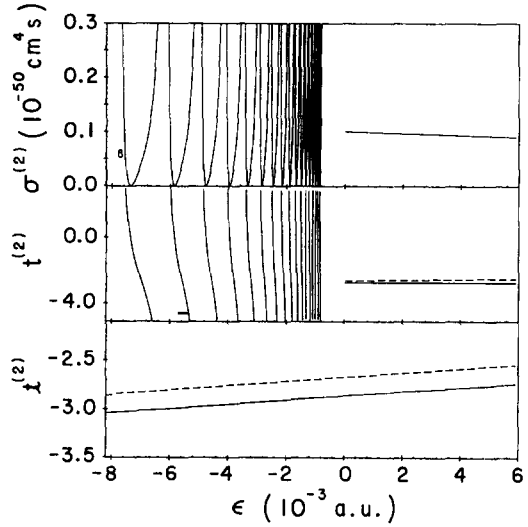

Fig. 6. Perturbative two-photon transition amplitude $T_{\mathrm{fi}}(E)$ for ionization of the hydrogen 1s state with circularly polarized light according to the quantum defect formula (39). The energy of the intermediate state is denoted ε. Top: Total generalized cross section $\sigma^{(2)}$. Center: Real (solid line) and imaginary (dashed line) part of $T_{\mathrm{fi}}(E)$. Bottom: Smooth quantum defect parameters [real and imaginary part of $T_{\mathrm{fi}}^{(\mathrm{s})}(E)$]. (From ref. [79])

generates a wave packet which escapes to infinity. The atom can only absorb a second photon from the probe laser, if the electron is still close to the ion core.

(ii) If the pump laser excites Rydberg states, in general there will be contributions from the first term and from the infinite sum, which stems from the resonant part of the two-photon amplitude. The first term contributes only for overlapping laser pulses. In this case the two-photon matrix element looks like in an above-threshold process when only continuum states are excited. This is related to the absence of intermediate Rydberg resonances in a two-photon process with spectrally broad pulses $\hbar/\tau_a$, $\hbar/\tau_b \gg \hbar/T_{E_{\bar{n}}}$ and $t_b \approx t_a$. The terms in the infinite sum give contributions for time delays $t_b - t_a \sim (M+1)T_{E_{\bar{n}}}(M = 0, 1, 2, \ldots)$. This reflects the repeated returns of the wave packet to the ionic core, where the electron can make a transition to the final state $|f\rangle$ by emitting a photon from the laser field. Evaluating the integrals appearing in eq. (40) in a stationary phase approximation we obtain for time delays with $t_b - t_a \gg \tau_a, \tau_b$,

$$P_{fi} = \left| \frac{1}{\hbar^2} \sum_{M=0}^{\infty} \sum_{lm} \mathscr{D}^{(+)}_{f,\varepsilon lm} \tilde{\mathscr{E}}^*_b(\delta^b_E) \mathscr{D}^{(-)}_{\varepsilon lm,i} \tilde{\mathscr{E}}_a(\delta^a_E) \right.$$
$$\left. \times [3(M+1)(-E/\mathscr{R}y)^{-5/2}(2\mathscr{R}y)^{-2}]^{-1/2} e^{i\pi/4} e^{i\phi(E)} \right|^2_{E=E_s^{(M)}}, \tag{41}$$

with

$$\phi(E) = \delta^a_E t_a - \delta^b_E t_b + 2\pi M \alpha_l + 2\pi(M+1)(-E/\mathscr{R}y)^{-1/2}.$$

The points of stationary phase, $E_s^{(M)}$, are determined by

$$\hbar \left. \frac{d\phi}{dE} \right|_{E=E_s^{(M)}} \equiv -(t_b - t_a) + (M+1)T_{E_s^{(M)}} = 0 \quad (M = 0, 1, 2, \ldots). \tag{42}$$

This stationary phase evaluation is valid as long as $\frac{1}{2}(d^2\Phi/dE^2)(\hbar/\tau_a)^2 \gg 1$. The dominant contribution to the sum of eq. (41) comes from stationary energies with $E_s^{(M)} \sim E_i + \hbar\omega_a \sim E_f + \hbar\omega_b$, so that the time delay between both pulses is a multiple of the mean classical orbit time. Figure 7 shows the two-photon

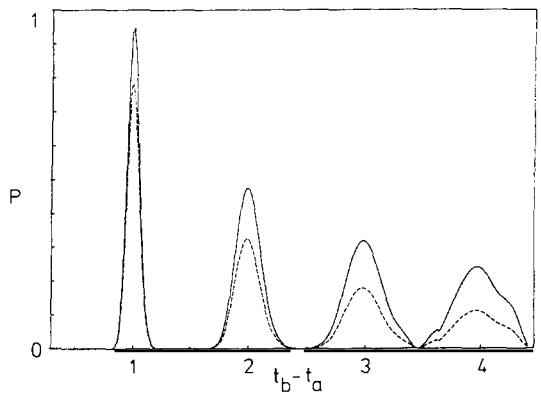

Fig. 7. Two-photon Raman transition probability versus time delay between both laser pulses $t_b - t_a$ (in units of the classical orbit time T), according to ref. [18]. The parameters are $\tau_a = \tau_b = 12$ ps, $\bar{n} = 85$ ($T = 94$ ps). Solid line: a single Rydberg series is excited. Dashed line: the wave packet is a superposition of autoionizing Rydberg states ($\tau = 0.075$, see section 4.1).

transition probability of hydrogen as a function of the time delay in units of the classical orbit time for $\tau_a = \tau_b = 12$ ps, $\bar{n} = 85$ ($T = 94$ ps), $l = 1$ [18].

As mentioned above in section 2.1, not only energy-normalized dipole matrix elements from low lying bound states to Rydberg states are slowly varying functions of energy but also those describing ionization from the Rydberg states. Thus, the ionization probability in a two-photon experiment with time-delayed pulses will show a structure similar to the Raman process discussed above [17]. The advantage of observing radial Rydberg wave packets in ionization is that only a single laser is needed, which generates a pump and a probe pulse. The disadvantage of a single-laser setup is that the ionized electrons created by both pulses have the same energy. Therefore the total ionization signal will not only consist of the contribution of the generated wave packet but also of the direct multiphoton ionization by the individual pulses.

Two experiments have reported observation of a radial Rydberg wave packet using pump–probe schemes with two-photon excitation of the wave packet and subsequent ionization in a single-laser setup. In the experiment of ref. [21] Rydberg states of Rb around 42d were excited with a 6 ps pulse and a central wavelength of 594.8 nm. The classical orbit time was 10.2 ps. The result for the ionization signal as a function of the time delay is given in fig. 8. The ionization signal due to the separate pulses is subtracted from the total signal. Around zero time delay the wave packet has not yet left the core and multiphoton ionization takes place by absorption of photons from both pulses. The coherent spike in the light intensity due to temporal and spatial overlap of the two pulses gives rise to the extra large peak in the ionization yield. With increasing time delay two peaks at approximately 9.4 ps and 18 ps are seen. They correspond to successive returns of the radial wave packet to the core region. Yeazell et al. [24, 25] used a 20 ps pulse to excite a coherent superposition of states around $n = 85$ in potassium. Results of the experiment and their comparison with theory are shown in fig. 9. The ion signal shows peaks at multiples of the classical orbit time of 107 ps. The decreasing height of the succeeding peaks is primarily due to pulse-to-pulse frequency fluctuations and partly also due to dephasing of the coherent superposition of states.

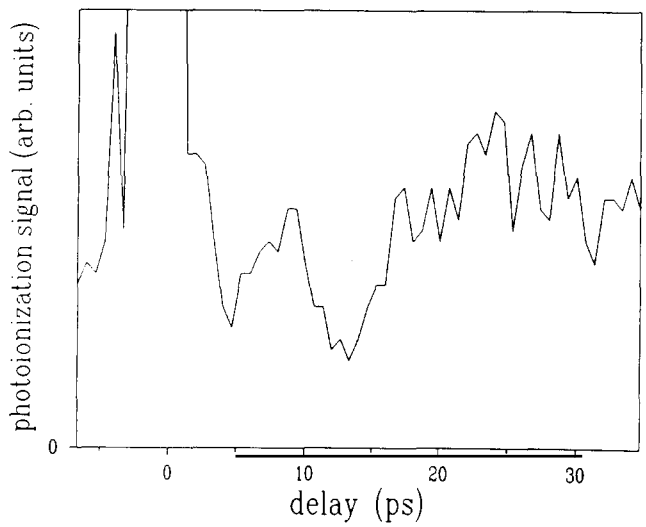

Fig. 8. Photoionization signal of the wave packet as a function of the time delay between pump and probe pulse (derived from a single laser) according to the experiment of ten Wolde et al. [21]. Rydberg states of rubidium were excited around the 42d state ($T = 10.2$ ps) with a 6 ps pulse. At 9 ps and 18 ps, the return of the wave packet to the core leads to an enhancement of the ion signal.

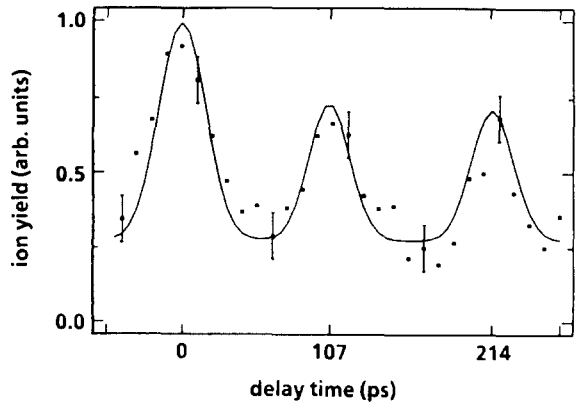

Fig. 9. Experimental and theoretical results for a photoionization signal in a pump–probe experiment (squares and solid curves, respectively) according to Yeazell et al. [25]. A single-laser setup was used; approximately five Rydberg states of potassium around $\bar{n} = 89$ ($T = 107$ ps) were excited by a 25 ps pulse.

We conclude by pointing out that according to ref. [27] even *incoherent* pump and probe pulses will lead to modulation patterns in the ionization probability as a function of time delay. The necessary conditions are that the coherence time of the incoherent light pulse has to be shorter than the classical orbit time and that pump and probe pulse are derived from the same light source. However, the pulse duration does not have to be shorter than the classical orbit time.

2.2.3. Generation by an intense laser field

In this section we study the excitation of a Rydberg series by an intense, not necessarily short laser pulse close to threshold (see fig. 2). By intense pulse we mean that the time scale of the atomic evolution, as induced by the laser light, can be shorter than the duration of the light pulse. This requires a nonperturbative solution of equations of the type of eq. (22) [28–37, 81–85]. Two cases will be discussed below: (i) the depletion time of the ground state is much shorter than the classical orbit time; (ii) the Stark shift of the Rydberg states is larger than the spectral width of the pulse and the energy spacing of the Rydberg levels. In the first case a radial wave packet is generated due to the rapid depletion of the ground state population. These *depletion wave packets* have been discussed in refs. [30, 32]. The second case is realized when a high-order multiphoton process excites electrons close to threshold [20, 37, 38]. Our derivations will again be based on quantum defect methods. This implies that the interaction with the Rydberg series is treated as a whole including the infinite number of Rydberg states and the adjoining continuum from the outset.

In a series of papers Fedorov and coworkers have studied strong field effects in coherent processes involving Rydberg states [28, 31, 35], predicting, for example, stabilization of Rydberg states in strong fields due to interference effects caused by Raman-type transitions via the continuum. The dynamics and quasi-energies of a system consisting of a ground state and a quasicontinuum of levels in a resonant external field has also been analyzed for the entire range of intensities and various rise times of the field by various authors [81–83] and has been extended recently to include laser band width effects [84]. Grochmalicki and Lewenstein [33] have discussed excitation of Rydberg wave packets by short laser pulses including saturation effects for a class of pulse shapes and have emphasized the importance of smoothness of the pulse.

To describe the formation of *depletion wave packets* we start from eqs. (21) and (22). Although for

strong fields one expects in general also other excitation channels to contribute, the problem studied below is the basic building block of more realistic models. We assume that the electric field of the laser is turned on instantaneously at $t = 0$ and that the envelope has the form of a square pulse with constant amplitude $\mathscr{E}(t) = \mathscr{E}$. However, the essential difference to subsection 2.2.1 is that a perturbative solution of the Schrödinger equation is no longer sufficient. To simplify notation, we consider only coupling to a single Rydberg series, i.e., we suppress the angular momentum quantum numbers lm, and use Hartree atomic units ($e = \hbar = M_e = 1$).

The Laplace transform of the initial-state amplitude $a_i(z)$ is defined by

$$a_i(t) = \frac{1}{2\pi} \int_{-\infty+i0}^{\infty+i0} dz\, e^{-izt} a_i(z)\,, \tag{43}$$

and is explicitly given by

$$a_i(z) = i[z - E_i - \Sigma(z+\omega)]^{-1}\,, \tag{44}$$

with the self-energy of the initial state $\Sigma(z) = T_{ii}(z)|\mathscr{E}|^2$. Before proceeding to a discussion of near-threshold phenomena, we find it worthwhile to review the solution of eq. (22) in the energy region far below and far above threshold.

Far below threshold (*the two-level approximation*). Whenever the laser pulse is tuned to near resonance with one of the bound states $|n\rangle$, i.e., $|E_i + \omega - E_n| \ll |E_n - E_{n\pm1}|$, and the intensity is sufficiently low, i.e., $|\Omega_n| = 2|\langle n|\boldsymbol{\mu}\cdot\boldsymbol{\varepsilon}|i\rangle\mathscr{E}| \ll |E_n - E_{n\pm1}|$, only state $|n\rangle$ is excited significantly. Therefore, the self-energy $\Sigma(z)$ may be approximated by keeping only the single state $|n\rangle$ in the spectral decomposition,

$$\Sigma(E) \sim \tfrac{1}{4}|\Omega_n|^2/(E - E_n)\,, \tag{45}$$

with the Rabi frequency Ω_n. Inserting eq. (45) into eq. (44) we find the poles, $z_{1,2}$, of $a_i(z)$ and the corresponding quasi-energies, $\tilde{E}_{1,2} = z_{1,2} + \omega$, from the quadratic equation

$$(\tilde{E} - \bar{E})(\tilde{E} - E_n) - \tfrac{1}{4}|\Omega_n|^2 = 0\,, \tag{46}$$

with the mean excited energy $\bar{E} = E_i + \omega$. These quasi-energies describe the positions of the Stark-split energy levels.

Inverting the Laplace transform of eq. (43) we obtain for the initial-state amplitude

$$a_i(t) = \sum_{j=1}^{2} e^{-i(\tilde{E}_j - \omega)t} \frac{(\frac{1}{2}|\Omega_n|)^2}{(\tilde{E}_j - \bar{E})^2 + (\frac{1}{2}|\Omega_n|)^2}\,. \tag{47}$$

The initial-state probability therefore exhibits the well-known Rabi oscillations with frequency $[(E_n - \bar{E})^2 + (\frac{1}{2}|\Omega_n|)^2]^{1/2}$.

Far above threshold (*exponential decay*). If the laser field is tuned well above the ionization

threshold, the dominant contribution to $\Sigma(z)$ comes from the excited continuum states near the energy conserving value $z + \omega = E \sim \bar{E}$. As the bound–free dipole matrix elements are smooth functions of energy, we may approximate $\Sigma(z + \omega)$ by its values near $z = E_i$ (pole approximation),

$$\Sigma(z + \omega) \sim \delta E_i - i\gamma/2 . \tag{48}$$

δE_i is an approximately energy independent quadratic Stark shift (which we assume to be absorbed in the initial-state energy E_i) and

$$\gamma = 2\pi |\langle \bar{E} | \boldsymbol{\mu} \cdot \boldsymbol{\varepsilon}\, \mathscr{E} | i \rangle|^2 \tag{49}$$

is the ionization rate in agreement with Fermi's golden rule. Thus the self-energy of eq. (48) gives rise to a complex quasienergy $\tilde{E} = z + \omega = \bar{E} - i\gamma/2$. Inverting the Laplace transform we find

$$a_i(t) = e^{-i(\bar{E} - \omega)t}\, e^{-\gamma t/2} , \tag{50}$$

and the initial-state probability is exponentially decaying as a function of time.

Near threshold. If the laser is tuned close to the photoionization threshold, many bound and continuum states contribute to the self-energy $\Sigma(z)$. Taking the Laplace transform of the wave function of eq. (21), we find the following system of close-coupling equations:

$$\begin{aligned} &(z - E_i) a_i(z) + \langle i | \boldsymbol{\mu} \cdot \boldsymbol{\varepsilon}^* \mathscr{E}^* | F(z + \omega) \rangle = i , \\ &(z + \omega - H_A) | F(z + \omega) \rangle + \boldsymbol{\mu} \cdot \boldsymbol{\varepsilon}\, \mathscr{E} | i \rangle a_i(z) = 0 . \end{aligned} \tag{51}$$

Solutions of similar equations, which describe the coupling between a bound channel $|i\rangle$ and a free channel $|F(z + \omega)\rangle$, have been studied in QDT [9]. Eliminating $|F(z + \omega)\rangle$ in eq. (51) we find for the self-energy ($E = I + \varepsilon$)

$$\Sigma(E) = \begin{cases} \delta\omega - i\gamma/2 & (\varepsilon > 0) , \\ \delta\omega + (\gamma/2) \cot[\pi(\nu + \alpha)] & (\varepsilon = -1/(2\nu^2) < 0) . \end{cases} \tag{52}$$

Here, $\delta\omega$ and γ are a quadratic Stark shift contribution and the ionization rate. The shift $\delta\omega$ is assumed to be absorbed in the initial state energy E_i together with the ponderomotive shift of the Rydberg threshold. As a consequence of the finite-range character of the radiative coupling (see sections 2.1 and 2.2.2), $\delta\omega$ and γ are approximately energy independent across threshold. The rapid energy dependence below threshold is contained in the cot term. $\Sigma(E)$ has poles at the Rydberg energies $\varepsilon_n = -\frac{1}{2}(n - \alpha)^{-2}$.

It is not difficult to see that eq. (52) reduces to the result of the two-level approximation when only a single state $|n\rangle$ is significantly excited. Near a resonance energy, $E \sim E_n$, we obtain eq. (45) provided we make the identification

$$\tfrac{1}{4} |\Omega_n|^2 = (\gamma/2\pi)(n - \alpha)^{-3} . \tag{53}$$

Note that eq. (53) implies the familiar $(n - \alpha)^{-3}$ scaling of the bound–Rydberg dipole matrix elements. Above threshold eq. (52) is identical with eq. (48).

Dressed energies, $\tilde{E}_n = z_n + \omega$, are determined by the poles of $a_i(z)$. According to eqs. (44) and (52), they are solutions of the transcendental equation

$$\tilde{E}_n = I - \frac{1}{2[n - \alpha - \mu(\tilde{E}_n)]^2}, \tag{54}$$

with the *intensity dependent* quantum defect

$$\mu(E) = (-1/\pi)\arctan[(\gamma/2)(E - \bar{E})^{-1}]. \tag{55}$$

The appearance of a Rydberg formula with a laser-induced quantum defect is not surprising: it is well known that the mixing of a bound state into the continuum leads to a resonant phase shift $\pi\mu(E)$; in the excitation from a low lying atomic state such a continuum phase shift manifests itself in the appearance of a laser-induced autoionizing-like resonance, whereas in the process of laser-assisted electron–ion scattering, which is described by the scattering matrix

$$\tilde{\chi}(E) = e^{2\pi i[\alpha + \mu(E)]}, \tag{56}$$

it gives rise to "capture–escape" resonances. On the other hand, in the bound state region scattering phase shifts correspond to quantum defects, in agreement with eq. (54).

We now return to study the time evolution of the initial-state amplitude. Using eq. (52) and inverting the Laplace transform by contour integration, we find the initial-state amplitude in the *dressed state representation*,

$$a_i(t) = \sum_n e^{-i(\tilde{E}_n - \omega)t} \frac{1}{\pi} \tilde{\nu}_n^{-3} \frac{\gamma/2}{(\tilde{E}_n - \bar{E})^2 + (\gamma/2)^2[1 + 2(\gamma\pi\tilde{\nu}_n^3)]}$$

$$+ \frac{i}{2\pi} e^{-i(\bar{E} - \omega)t}\{e^{-\gamma t/2}[E_1(-i\bar{E}t - \gamma t/2) - 2\pi i\Theta(\bar{E})] - e^{\gamma t/2}E_1(-i\bar{E}t + \gamma t/2)\}. \tag{57}$$

$\Theta(x)$ is the unit step function, which vanishes for $x < 0$. $E_1(x)$ is the exponential integral [86]. Equation (57) shows that all quasi-energies in an energy interval of width $\gamma[1 + 2/(\gamma\pi\bar{\nu}^3)]^{1/2}$ around the mean excited energy $\bar{E}$ contribute significantly to the excitation process. We can, therefore, distinguish between two different dynamical regimes, namely the two-level (or weak-field) limit characterized by $\gamma \ll \bar{\nu}^{-3}$, and the threshold (or intense-field) limit $\gamma \gg \bar{\nu}^{-3}$. The last case implies that for $\bar{E} < I$

$$T_{\bar{E}} = 2\pi[2(I - \bar{E})]^{-3/2} \gg 2\pi/\gamma, \tag{58}$$

with the classical orbit time of an electron in a Coulomb potential $T_{\bar{E}}$. In the time domain the inequality (58) expresses the fact that the laser-induced depletion time of the initial state, $1/\gamma$, is shorter than the classical orbit time of the excited electron.

Under condition (58) a direct evaluation of the sum of eq. (57) is inconvenient, because many dressed states contribute. Instead, we prefer to represent the initial-state amplitude in the form of a

classical path representation,

$$a_i(t) = e^{-i(\bar{E}-\omega)t} e^{-\gamma t/2} + \sum_{M=0}^{\infty} \int_{-\infty}^{I} dE\, e^{-i(E-\omega)t} [i(E - \bar{E} + i\gamma/2)^{-1} \mathscr{D}_{i,E}^{(+)} \mathscr{E}^*] e^{2\pi i\nu}$$

$$\times [\tilde{\chi}(E) e^{2\pi i\nu}]^M [\mathscr{D}_{E,i}^{(-)} \mathscr{E} i(E - \bar{E} + i\gamma/2)^{-1}], \tag{59}$$

with the photoionization and recombination dipole matrix elements

$$\mathscr{D}_{E,i}^{(-)} = -i e^{i\pi\alpha} \langle E | \boldsymbol{\mu} \cdot \boldsymbol{\varepsilon} | i \rangle , \qquad \mathscr{D}_{i,E}^{(+)} = -i e^{i\pi\alpha} \langle i | \boldsymbol{\mu} \cdot \boldsymbol{\varepsilon}^* | E \rangle$$

Compare with eqs. (11) and (12)] and the electron–ion scattering matrix $\tilde{\chi}(E)$. Since $\gamma \gg \bar{\nu}^{-3}$, $e^{2\pi i\nu}$ is a rapidly oscillating function of energy. Therefore, the dominant contribution to the energy integrals comes from points of stationary phase, $E_s^{(M)}$, which fulfill the relation $t = (M+1) T_{E_s^{(M)}}$, $M = 0, 1, 2, \ldots$. Performing the energy integration in eq. (59) with the stationary phase method we find

$$a_i(t) = e^{-i(\bar{E}-\omega)t} e^{-\gamma t/2}$$

$$+ \sum_{M=1}^{\infty} \left(\frac{2\pi}{|\partial^2 \Phi / \partial E^2|_{(M,t)}} \right)^{1/2} e^{i\pi/4} e^{i\Phi(E,M,t)} (\gamma/2\pi) [(E - \bar{E})^2 + (\gamma/2)^2]^{-1} \Big|_{E = E_s^{(M)}} , \tag{60}$$

with the phase $\Phi(E, M, t) = -(E - \omega)t + 2\pi M[\nu + \alpha + \mu(E)]$.

For a given time t the only contributing terms in eq. (60) are those for which $|E_s^{(M)} - \bar{E}| \leq \gamma$. Therefore, for times much shorter than the classical orbit time there are no stationary phase contributions and the initial-state amplitude decays exponentially with rate γ. The depletion of the initial state $|i\rangle$ on a time scale of the order of $1/\gamma \ll T_{\bar{E}}$ implies the generation of a radial electronic wave packet. The exponential decay law for the initial state for times $t \ll T_{\bar{E}}$ reflects the fact that the electronic motion is not affected by the outer turning point of the Coulomb potential and behaves like in a true ionization process above threshold. For times $t \sim T_{\bar{E}}$, the dominant contribution of eq. (60) stems from the term with $M = 1$, which describes the first return of the electronic wave packet to the inner turning point of its orbit. Inside the core region, the electron is scattered in the presence of the laser field and can be de-excited back to the initial state $|i\rangle$. Similar arguments can be presented for times $t \sim M T_{\bar{E}}$ $(M = 2, 3, \ldots)$, so that the population of the ground state will show population pulsations with the period of the classical orbit time.

Figures 10 show the initial-state probability as a function of time for different mean excited energies $\bar{\varepsilon}$ and a fixed value of γ and $\alpha = 0$. Figure 10a represents a case where only a few quasi-energies contribute in eq. (57), giving rise to slightly modified Rabi oscillations. As soon as the mean ionization time, $1/\gamma$, becomes comparable to or smaller than the classical orbit time, $T_{\bar{E}}$, the time dependence of the initial-state probability changes drastically (figs. 10b–d). In fig. 10c many Rydberg states are excited and a radial Rydberg wave packet is generated. Thus the ground state population shows population pulsations with the classical orbit time. The broadening of the recombination peaks reflects the spreading of the wave packet. For long times, when the wave packet is no longer well defined, the ground state population shows rapid oscillations. An extreme case is shown in fig. 10d, where Rydberg and continuum states are significantly excited. The excited energies correspond to orbit times from

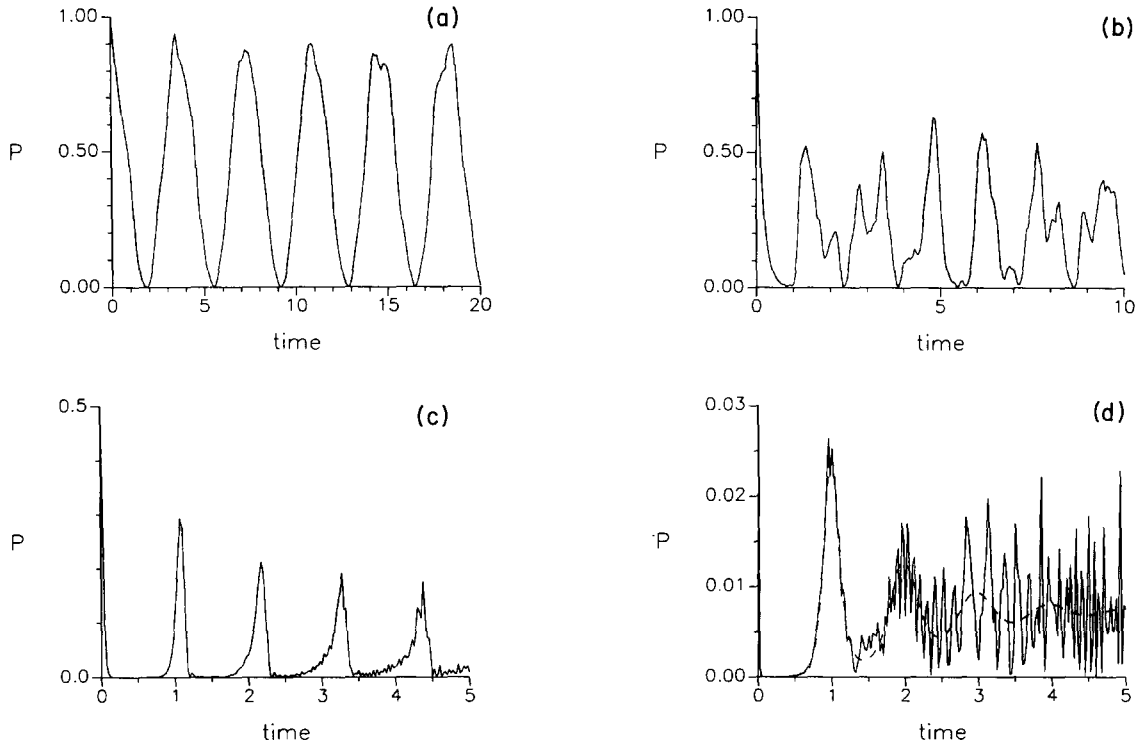

Fig. 10. Initial state probability, P, as a function of time (in units of the mean orbit time $T_{\bar{E}}$) for excitation of a Rydberg series with $\gamma = 4.13 \times 10^{10}\,s^{-1}$, (a) $\bar{\varepsilon} = -2 \times 10^{-4}$ au, (b) $\bar{\varepsilon} = -5 \times 10^{-5}$ au, (c) $\bar{\varepsilon} = -1.25 \times 10^{-5}$ au, (d) $\bar{\varepsilon} = -4 \times 10^{-6}$ au. The dashed curve in (d) shows the mean (time-averaged) initial-state probability.

some $T_{\min}$ up to infinity, so that the radial wave packet is not well defined. This leads to rapid oscillations, which correspond to the interference between contributions associated with different returns of the electron to the core region. Averaging over these oscillations one can show that in the present model the ground state population approaches a nonzero population in the long time limit. This value is approached asymptotically according to a power law involving $t^{-5/3}$ [29, 30].

Effects of the Stark shift. We have already discussed aspects regarding the Stark shift of atomic levels in subsection 2.2.1. We conclude this section with remarks on the threshold behavior of N-photon resonant $(N+1)$-photon ionization processes (typically $N = 3, 4, \ldots$) in cases where the Stark shift is much larger than the Fourier width of the pulse, so that it is the dominant broadening mechanism. Examples are multiphoton ionization experiments in rare gases [20]. Typically, in this case the shift of the ground state is small while the photoionization threshold is shifted upwards according to eq. (35). For an explanation of the experimentally observed threshold structure of ref. [20], inclusion of the time and space dependence of the ionizing laser pulse is of central importance. If the laser is tuned sufficiently far below threshold, the spectral width of the laser pulse is smaller than the Rydberg level spacing and the Rydberg states appear as isolated intermediate resonances. Close to threshold the energy level separation becomes smaller than the spectral width of the laser pulse and the resonance structure disappears. There are three time scales in the problem, the time scale associated with the Stark shift δE, the laser pulse duration τ_p and the classical orbit time T. (Note, however, that for a fixed

excitation energy there is an ambiguity in defining a Rydberg energy spacing, because the effective ionization threshold varies according to the space and time dependence of the laser field.) In figs. 11 the experimental and theoretical ionization probability of (2 + 1)-photon ionization of rubidium is shown as a function of laser frequency [87]. According to these figures, a region where individual Rydberg resonances are well resolved, is followed by a smoothly decreasing ionization probability in the bound-state region and an almost energy independent above-threshold ionization signal.

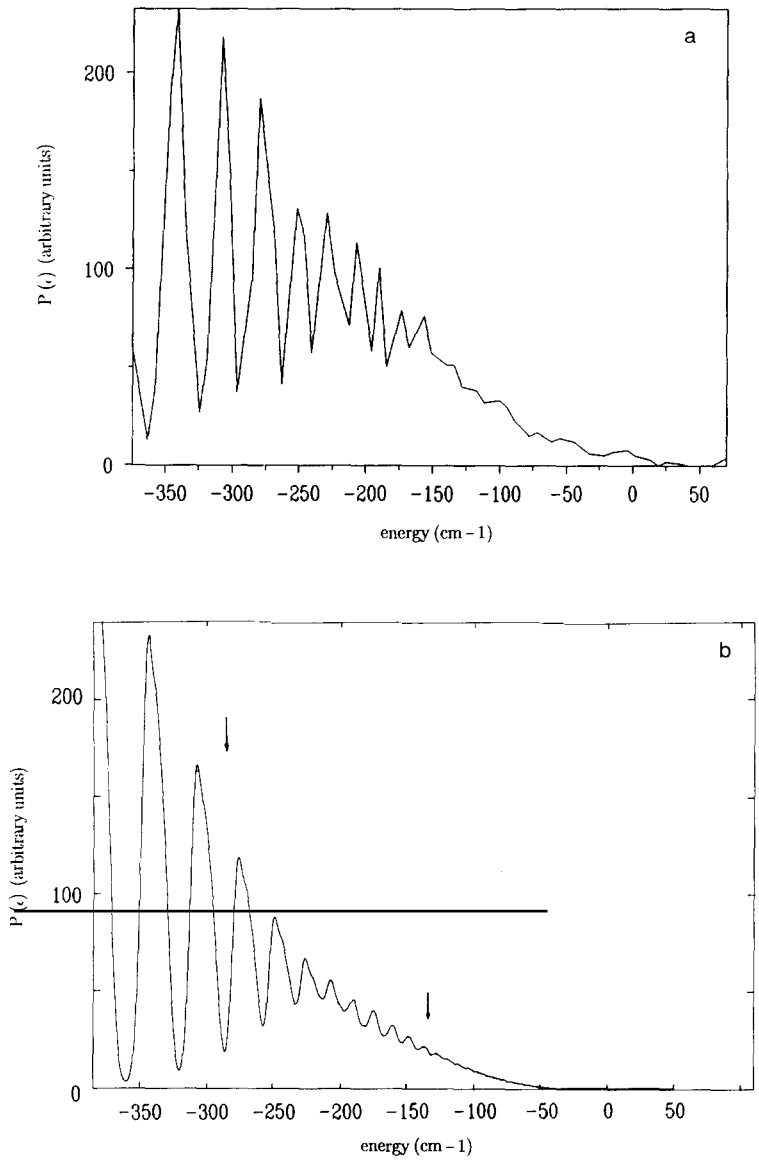

Fig. 11. Ionization probability of rubidium as a function of the laser frequency across threshold according to ref. [87]. The duration of the laser pulse is $\tau_p = 3.54$ ps, the maximum light intensity is $I = 6.9 \times 10^{10}$ W/cm^2. The two subplots are (a) experiment and (b) theory (for a Gaussian laser pulse). The left arrow on (b) (between the 20d and 21d states) indicates the position where the Stark shift equals the energy separation between the Rydberg levels. The right arrow corresponds to the position where the laser pulse duration is equal to the classical orbit time.

2.3. Angular Rydberg wave packets

An angular wave packet is a coherent superposition of energy eigenstates with high values of the angular momentum quantum numbers lm so that the polar and azimuthal angles of the excited electron are localized. Due to angular momentum selection rules, formation of such a superposition cannot be achieved by one- or two-photon absorption from an atomic ground state with a short laser pulse alone. Additional external fields or a special preparation of the atom is required for the excitation of high angular momentum states [46–48]. Although such an excitation is difficult to achieve experimentally, special properties of these high angular momentum states, for example their long radiative life times, their large electric and magnetic dipole moments and their anisotropic behavior in collisions, have motivated experimental efforts. Examples are the Stark excitation schemes of Hulet and Kleppner [46], the method of crossed electric and magnetic fields proposed by Delande and Gay [57] and the suggestion by Molander et al. [40] to employ dressing by a radio frequency field.

In a series of papers, Stroud and coworkers [24, 40–42] investigated the excitation of an angular wave packet consisting of a superposition of a large number of aligned Rydberg states with $m = l \gg 1$ and the same value of the principal quantum number, n, theoretically and experimentally. The wave function of such a state is given by $\Psi(r, \Theta, \Phi, t) = \Sigma_l A_l Y_l^l(\Theta, \Phi)\, e^{-iE_{nl}t/\hbar}$. Because $Y_l^l(\Theta, \Phi) \propto (\sin \Theta)^l$, the probability distribution of each of these aligned states is essentially confined to a plane perpendicular to the axis of quantization. A linear superposition of different l-values produces a localization with respect to the angle Φ. The time evolution of such an angular wave packet is determined by the interference between states with different angular momenta but a fixed value of n. For a nonrelativistic hydrogen atom these eigenstates are degenerate and the corresponding wave packet is stationary. In the case of alkali atoms, corrections to the $1/r$ Coulomb potential include a $1/r^4$ contribution from core polarization and relativistic effects. As a consequence, the wave packet will precess. This is in complete analogy to the precession of Mercury due to relativistic effects. As an example, fig. 12 shows the evolution of an angular wave packet according to Yeazell [24].

Following the suggestion of Molander et al. [40], in a recent experiment Yeazell and Stroud [42] prepared an angular wave packet by optical excitation of Rydberg states which are strongly dressed by a radio frequency (rf) field. Thereby a circularly polarized laser field excites electrons from the sodium ground state via two-photon absorption to the $n = 50$ d-state. The $n = 50$ manifold is dressed by a circularly polarized rf field (frequency 65 MHz, field strength 0.3 V/cm), which is tuned near the thirty-photon resonance between the states $(n, l) = (50, 2)$ and $(n, l) = (50, 32)$. As a consequence this high angular momentum state and several of its neighbors are strongly mixed with the 50d state. All of these rf-dressed levels lie within the coherent band width of the short optical pulse (pulse duration $\tau_p = 500$ ps). Turning off the rf field adiabatically, the population in the dressed states goes directly into the angular momentum eigenstates with which they are connected, leaving a coherent superposition of l-states. After the rf field is turned off, the motion of the (free) wave packet is due to core polarization and relativistic effects. Detection of this angular wave packet is achieved by ionization with a pulsed electric field. The ionization signal depends on time and the angular localization of the wave packet. A wave packet aligned in the direction of the ionizing field has a larger ionization rate than one aligned in another direction. Therefore, the time dependence of the ionization signal provides a signature of the orientation of the wave packet. Yeazell and Stroud [42] performed a classical Monte Carlo calculation to model this ionization process. Very good agreement is achieved with their experimental results, demonstrating the experimental realization of an angular wave packet. Precession of the wave packet has so far not been observed experimentally because of the long precession times, which are typically of the order of milliseconds.

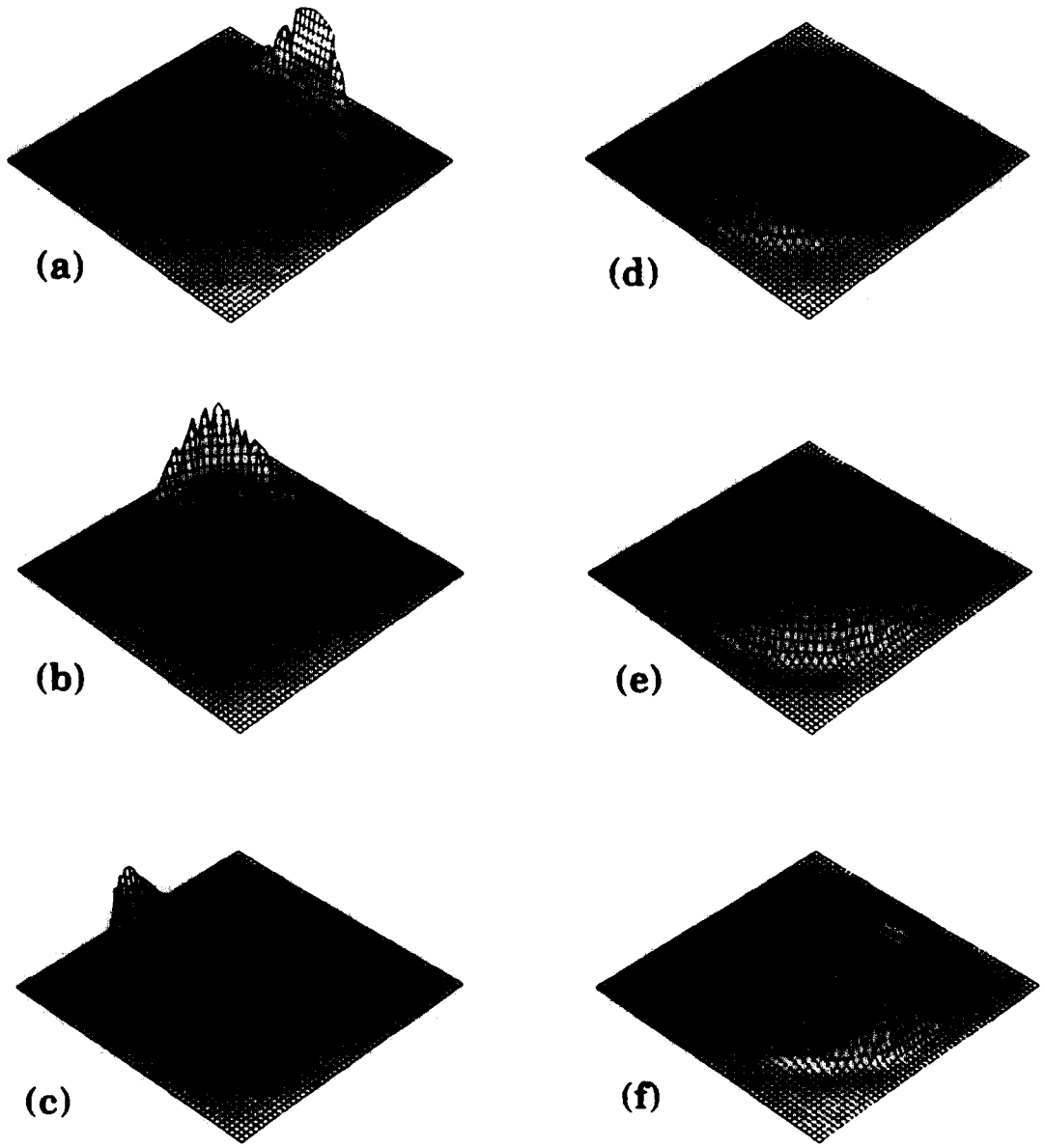

Fig. 12. Evolution of an angular wave packet according to Yeazell [24]. After the dressing radio frequency field has been turned off, the probability density of the wave packet is shown at intervals of 56 μs. The wave packet is described by a three-dimensional plot of the probability density in the plane perpendicular to the axis of quantization. The wave packet precesses due to perturbations of the Coulomb potential with period $T = 340$ μs.

Coherent excitation of a superposition of DC-Stark-split atomic states has been reported recently in ref. [43]. For small static electric field strengths F, the Stark shift of an alkali Rydberg state scales linearly with F. For hydrogen the energies of the Stark-split states are given by $E_{n_1 n_2} = -\mathcal{R}y/n^2 + 3\mathcal{R}y(F/F_0)n(n_1 - n_2)$ with the principal quantum number $n = n_1 + n_2 + m + 1$, the parabolic quantum numbers n_1, n_2 and the atomic unit of electric field strength $F_0 = 5.14 \times 10^{11}\ \mathrm{V\,m^{-1}}$. Therefore, coherent laser excitation of these energy levels leads to a beating period $T = (\hbar/2\mathcal{R}y)(2\pi)/[\frac{3}{2}(F/F_0)n]$,

which is the same for all neighboring components. These Stark states are superpositions of angular momentum eigenstates. According to calculations in ref. [43], a wave packet consisting of a superposition of such Stark states is oscillating between a more or less spherical distribution of low-l states and a distribution which is strongly oriented along the electric-field axis. In ref. [43], the periodic motion of such a wave packet was observed in Rb for excitation of Rydberg states with $n = 23$ in a single-laser setup with pulse duration $\tau_p = 5$ ps. The Stark period was $T = 45.8$ ps. The observed modulations of the ionization signal reflect the oscillations of the electronic charge distribution.

Recently, it has been shown by Delande and Gay [57] how in the presence of weak, static electric and magnetic fields a stationary hydrogenic energy eigenstate can be excited which is localized on a Kepler ellipse with minimum quantum fluctuations. This excitation scheme certainly constitutes a promising step towards the final goal of preparing a localized electronic wave packet which moves along a Kepler orbit. Experimentally, excitation of such a minimum uncertainty energy eigenstate has been demonstrated recently by Hare et al. [48]. For the preparation of an ideal Kepler wave packet a superposition of many of these energy eigenstates is needed. These minimum uncertainty energy eigenstates might have interesting spectroscopic applications in the future. They are discussed in more detail in section 3.2.

3. Theoretical methods and aspects

The purpose of this and the following chapter is (i) to generalize the treatment of the single-channel Coulomb case of chapter 2 to the many-electron (many-channel) problem and (ii) to discuss wave packet dynamics in the presence of external static fields. Theoretical methods based on Multichannel Quantum Defect Theory (MQDT) and semiclassical techniques are developed in this chapter, whereas physical applications are postponed to chapter 4. We conclude this chapter with a brief discussion of the minimum-uncertainty states of the Kepler problem.

In this and in the following chapter we shall use Hartree atomic units with $e = M_e = \hbar = 1$.

3.1. Classical path representation of atomic transition amplitudes

Recently, there has been renewed interest in the description of atomic and molecular laser excitation processes with semiclassical techniques [88–98] in which quantum mechanical wave functions and observables are constructed directly from properties of the trajectories of the corresponding classical problems [88, 92, 95–98]. These methods clearly exhibit the connections between classical dynamics and quantum mechanics and their application is particularly interesting in cases where the classical dynamics is not integrable and exhibits complicated phase space structure. Recently, these methods have also been applied to the description of laser excitation processes of atomic Rydberg states close to a photoionization threshold [17, 18, 30, 32, 34, 36, 99, 100].

For highly excited Rydberg states with small values of the angular momentum the classically accessible region of configuration space is large in comparison with the Bohr radius. This implies large classical actions. Therefore, semiclassical methods are applicable for the description of these states and classical path representations may be derived in which the atomic transition amplitudes of interest are expressed as a sum of contributions of all closed orbits of the excited Rydberg electron, which start from the nucleus. In the context of laser excitation of Rydberg states close to a photoionization threshold such representations have been derived recently for an unperturbed atom in refs. [17, 18, 30,

32] and for an atom in a static external field in refs. [34, 36, 99, 100]. These classical path representations are particularly useful for the description of the dynamics of radial Rydberg wave packets and are derived in the following. In the special case of a one-channel Coulomb problem, such classical path representations have already been encountered in chapter 2.

As has been shown in section 2.2, the quantity of central importance in atomic processes which involve resonant absorption and stimulated emission of laser radiation (within perturbation theory), is the resonant part of the two-photon transition amplitude as given in eq. (38),

$$T_{\mathrm{fi}}(\varepsilon) = \langle \mathrm{f}|\boldsymbol{\mu}\cdot\boldsymbol{\varepsilon}_{\mathrm{b}}^{*}(\varepsilon - H_{\mathrm{A}} + \mathrm{i}0)^{-1}\boldsymbol{\mu}\cdot\boldsymbol{\varepsilon}_{\mathrm{a}}|\mathrm{i}\rangle \quad (\varepsilon \sim \varepsilon_{\mathrm{i}} + \omega_{\mathrm{a}})\,, \tag{61}$$

between an initial state $|\mathrm{i}\rangle$ with energy ε_{i} and a final state $|\mathrm{f}\rangle$. H_{A} is the atomic Hamiltonian, μ is the atomic dipole operator and $\boldsymbol{\varepsilon}_{\mathrm{a}}$, $\boldsymbol{\varepsilon}_{\mathrm{b}}$ and ω_{a}, ω_{b} are the polarizations and frequencies of the absorbed and emitted laser photons. With the replacement $\boldsymbol{\varepsilon}_{\mathrm{b}}^{*} \rightarrow \boldsymbol{\varepsilon}_{\mathrm{b}}$, eq. (61) also describes one-photon resonant two-photon absorption. The main problem in the description of such laser excitation processes is the determination of the energy dependence of $T_{\mathrm{fi}}(\varepsilon)$. This problem has been discussed for the single-channel case in subsection 2.2.2.

In terms of this two-photon transition amplitude the final-state probability of the two-photon Raman excitation process of subsection 2.2.2 is given in eq. (37). In the special case of one-photon excitation from an energetically low lying bound state $|g\rangle$, the resonant part of the self-energy is related to this two-photon transition amplitude by

$$\Sigma(\varepsilon) = T_{gg}(\varepsilon)|\mathscr{E}|^{2}\,, \tag{62}$$

with $\boldsymbol{\varepsilon}_{\mathrm{a}} = \boldsymbol{\varepsilon}_{\mathrm{b}}$. Its imaginary part gives the one-photon excitation rate,

$$\Gamma = -2\,\mathrm{Im}\,[\Sigma(\varepsilon)]_{\varepsilon=\varepsilon_{g}+\omega}\,, \tag{63}$$

which describes the laser-induced depletion of state $|g\rangle$ in the limit where the depletion time $1/\Gamma$ is much larger than the pulse duration τ_{p} [compare with eq. (52)].

The generalization of eq. (39) to the many-channel case is conveniently done using the Dalgarno–Lewis method [101]. The two-photon transition amplitude is related to the solution $|F_{\varepsilon}\rangle$ of the inhomogeneous Schrödinger equation

$$(\varepsilon - H_{\mathrm{A}} + \mathrm{i}0)|F_{\varepsilon}\rangle = \boldsymbol{\mu}\cdot\boldsymbol{\varepsilon}_{\mathrm{a}}|\mathrm{i}\rangle \tag{64}$$

by

$$T_{\mathrm{fi}}(\varepsilon) = \langle \mathrm{f}|\boldsymbol{\mu}\cdot\boldsymbol{\varepsilon}_{\mathrm{b}}^{*}|F_{\varepsilon}\rangle\,. \tag{65}$$

It can therefore be evaluated in two steps: In a first step we solve the inhomogeneous Schrödinger equation (64) and in a second step we determine the dipole matrix element between the final state $|\mathrm{f}\rangle$ and the excited atomic state $|F_{\varepsilon}\rangle$ as given by eq. (65).

The main purpose of this section is the derivation of classical path representations for the two-photon transition amplitude with the help of this method. In subsection 3.1.1 we concentrate on an unperturbed atom, where at large distances from the nucleus the dynamics of the excited electron is

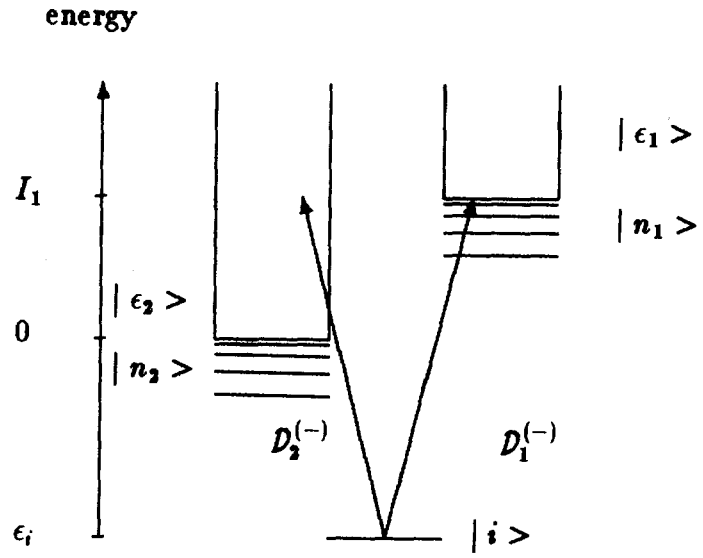

Fig. 13. Schematic representation of laser excitation of autoionizing Rydberg states.

determined by the $(1/r)$ Coulomb potential of the ionic core and we generalize the results of eq. (39) to the case of many fragmentation channels as schematically indicated in fig. 13. In this case, a classical path representation may be derived from standard results of QDT [18, 30, 32]. In subsection 3.1.2 we generalize these results to cases where at large distances from the nucleus the dynamics of the excited electron is modified, for example, by a static external field. Under these conditions a classical path representation may be derived with the help of multidimensional semiclassical methods [36, 99, 100].

3.1.1. The multichannel Coulomb problem

If one of the outer electrons of an atom with several valence electrons (an alkaline earth atom, for example [11]) is excited by a laser pulse, it may exchange energy with the ionic core. In the framework of an independent particle model the energy spectrum of the neutral atom consists of Rydberg series converging to various fragmentation thresholds with energies I_j. Due to electron correlation effects these Rydberg series and continua are coupled, and energy is exchanged between them [9, 14].

In an N-channel approximation, a solution of the homogeneous part of eq. (64) is given by

$$\psi_\varepsilon(R, r) = \sum_{j=1}^{N} \Phi_j(R) \frac{1}{r} F_j(\varepsilon, r) . \tag{66}$$

The channel functions, $\Phi_j(R)$, characterize the state of the ionic core with R indicating its coordinates and the angular momentum and spin of the excited electron. In the nonrelativistic approximation the radial wave function of the excited electron is determined by [9, 18, 30, 79]

$$\sum_{k=1}^{N} [(\varepsilon_j - h_j(r))\delta_{jk} - V_{jk}(r)] F_k(\varepsilon, r) = q_j(r) \quad (j = 1, \ldots, N) . \tag{67}$$

The energy of the excited electron in fragmentation channel j is $\varepsilon_j = \varepsilon - I_j$. If $\varepsilon_j < 0$, fragmentation

channel j is closed, otherwise it is open. The radial Hamiltonian of the excited electron, $h_j(r)$, includes the long-range $(1/r)$ Coulomb potential of the ionic core and is given by

$$h_j(r) = -\frac{1}{2}\left(\frac{\mathrm{d}^2}{\mathrm{d}r^2} - \frac{l_j(l_j+1)}{r^2}\right) - \frac{1}{r}\,.$$

The residual potential, $V_{jk}(r)$, describes the electron-correlation-induced coupling between the fragmentation channels and $q_j(r) = r\langle \Phi_j | \boldsymbol{\mu}\cdot\boldsymbol{\varepsilon}_a | \mathrm{i}\rangle_r$ describes laser-induced excitation from the initial state $|\mathrm{i}\rangle$.

As far as the dynamics of the excited electron is concerned, we may distinguish two characteristic physical regions:

1. For nonhydrogenic ionic cores the potential $V_{jk}(r)$ tends to zero at least as $1/r^3$ at large distances from the core. It may therefore be treated approximately as a finite-range coupling, which is restricted to a *reaction zone* of a few Bohr radii around the atomic nucleus, i.e., $V_{jk}(r) = 0$ for $r > r_c \sim 1$ [9, 14]. The energetically low lying bound state $|\mathrm{i}\rangle$ is also localized in a region of this size around the atomic nucleus so that we have $q_j(r) = 0$ for $r > r_c$, approximately.

2. Therefore, outside the reaction zone the dynamics of the excited electron is determined by the $(1/r)$ Coulomb potential of the ionic core and eq. (67) may be solved analytically.

For energies above all thresholds, i.e., $\varepsilon_j > 0$ ($j = 1, \ldots, N$), and large values of r the physical solution of eq. (67), which is regular for $r \to 0$ and remains finite for $r \to \infty$, is given by [18, 30]

$$F_j^{(\mathrm{p})}(\varepsilon, r) \sim -\varphi_{l_j}^{(+)}(\varepsilon_j, r)\mathrm{i}\pi\mathscr{D}_j^{(-)} \quad (1 \ll r)\,. \tag{68}$$

The photoionization dipole matrix element

$$\mathscr{D}_j^{(-)} = \sum_{k=1}^{N} \int_0^\infty \mathrm{d}r\, [\mathscr{F}_{kj}^{(-)}(\varepsilon, r)]^* q_k(r) \tag{69}$$

describes laser-induced excitation of channel j. The solution $\mathscr{F}_{kj}^{(-)}(\varepsilon, r)$ of the homogeneous part of eq. (67) describes an electron leaving the ionic core in channel j and behaves asymptotically as

$$\mathscr{F}_{kj}^{(-)}(\varepsilon, r) \sim \tfrac{1}{2}[\varphi_{l_k}^{(+)}(\varepsilon_k, r)\delta_{kj} - \varphi_{l_k}^{(-)}(\varepsilon_k, r)\chi_{kj}^*] \quad (1 \ll r)\,, \tag{70}$$

with the energy-normalized outgoing and incoming Coulomb functions $\varphi_{l_j}^{(\pm)}(\varepsilon_j, r)$ [9], respectively. Semiclassically, they are given by

$$\varphi_{l_j}^{(\pm)}(\varepsilon_j, r) \sim \sqrt{2/[\pi p(r)]}\,\exp\{\pm\mathrm{i}[w_{\varepsilon_j}(r_1, r) - (l_j + 1/2)\pi + \pi/4]\} \quad (r_1 \ll r \ll r_2)\,, \tag{71}$$

with the classical action $w_{\varepsilon_j}(r_1, r)$, the turning point r_1 and the radial momentum $p(r) = [2(\varepsilon_j + 1/r)]^{1/2}$. The scattering matrix elements χ_{kj} describe electron scattering between channels k and j, which takes place inside the reaction zone due to the presence of the residual electrons. These matrix elements are smooth functions of energy across any threshold [9, 14].

For some channels closed, i.e., $\varepsilon_j < 0$ ($j = 1, \ldots, N_c < N$), $F_j^{(\mathrm{p})}(\varepsilon, r)$ as given in eq. (68) diverges for $r \to \infty$. However, in this case the physical solution of eq. (67) is given by a linear combination of the

particular solution $F_j^{(\mathrm{p})}(\varepsilon, r)$ and a solution of the homogeneous part of eq. (67), i.e.,

$$F_j(\varepsilon, r) = F_j^{(\mathrm{p})}(\varepsilon, r) + \sum_{k=1}^{N} [\mathscr{F}_{jk}^{(-)}(\varepsilon, r)]^* \mathscr{A}_k(\varepsilon) . \tag{72}$$

The amplitudes $\mathscr{A}_k(\varepsilon)$ are determined by the requirement that $F_j(\varepsilon, r)$ has to remain finite for $r \to \infty$. Using well-known properties of the Coulomb functions $\varphi_{l_j}^{(\pm)}(\varepsilon_j, r)$ [9] or of their semiclassical approximations, we find

$$\mathscr{A}_k(\varepsilon) = \begin{cases} \sum_{j=1}^{N_c} [\mathrm{e}^{2\mathrm{i}\pi\nu_c}(1 - \chi_{cc}\,\mathrm{e}^{2\mathrm{i}\pi\nu_c})^{-1}]_{kj} 2\mathrm{i}\pi \mathscr{D}_j^{(-)} & (k = 1, \ldots, N_c) , \\ 0 & (k = N_c + 1, \ldots, N) . \end{cases} \tag{73}$$

The matrix χ_{cc} is the scattering matrix in the closed-channel subspace and $\mathrm{e}^{2\mathrm{i}\pi\nu_c}$ is the diagonal matrix with elements $\mathrm{e}^{2\mathrm{i}\pi\nu_j}$ and $\nu_j = (-2\varepsilon_j)^{-1/2}$. Inserting eqs. (72) and (73) into eq. (65) we obtain the two-photon transition amplitude

$$T_{\mathrm{fi}}(\varepsilon) = T_{\mathrm{fi}}^{(\mathrm{s})} + 2\mathrm{i}\pi \sum_{j,k=1}^{N_c} \mathscr{D}_j^{(+)} [\mathrm{e}^{2\mathrm{i}\pi\nu_c}(1 - \chi_{cc}\,\mathrm{e}^{2\mathrm{i}\pi\nu_c})^{-1}]_{jk} \mathscr{D}_k^{(-)} , \tag{74}$$

with the recombination dipole matrix element

$$\mathscr{D}_j^{(+)} = \sum_{k=1}^{N} \int_0^{\infty} \mathrm{d}r\, \langle \mathrm{f} | \boldsymbol{\mu} \cdot \boldsymbol{\varepsilon}_{\mathrm{f}}^* | \Phi_k \rangle_r [\mathscr{F}_{kj}^{(-)}(\varepsilon, r)]^* . \tag{75}$$

The first term of eq. (74) describes the "direct" two-photon transition, which takes place inside the reaction zone. Above all thresholds this is the only contribution to $T_{\mathrm{fi}}(\varepsilon)$. The residual terms of eq. (74) describe the resonant contributions from the Rydberg states. If $|\mathrm{f}\rangle$ is an energetically low lying bound state, the reaction zone extends only a few Bohr radii around the atomic nucleus and $T_{\mathrm{fi}}^{(\mathrm{s})}$ and the photoionization and recombination dipole matrix elements $\mathscr{D}_j^{(-)}$ and $\mathscr{D}_j^{(+)}$ are slowly varying functions of energy across any threshold [9, 14]. If the second laser pulse induces a transition from highly excited Rydberg states to continuum states well above threshold, the effective range of the radiative coupling r_c may be estimated by the distance the Rydberg electron can move away from the nucleus during the absorption of the laser photon. This characteristic absorption time is of order $\tau \sim \omega^{-1}$, which implies $r_c \sim \omega^{-2/3}$ [78]. Therefore, in the optical frequency regime photoabsorption from highly excited Rydberg states is also localized in space in a finite reaction zone around the atomic nucleus so that even in this case $T_{\mathrm{fi}}^{(\mathrm{s})}$, $\mathscr{D}_j^{(-)}$ and $\mathscr{D}_j^{(+)}$ are slowly varying functions of energy across threshold (compare also fig. 1 and the corresponding discussion in section 2.1).

Expanding eq. (74) in a geometric series we finally obtain the *classical path representation* [17, 18, 30]

$$T_{\mathrm{fi}}(\varepsilon) = T_{\mathrm{fi}}^{(\mathrm{s})} + 2\mathrm{i}\pi \sum_{j,k=1}^{N_c} \mathscr{D}_j^{(+)} \sum_{M=0}^{\infty} [\mathrm{e}^{2\mathrm{i}\pi\nu_c}(\chi_{cc}\,\mathrm{e}^{2\mathrm{i}\pi\nu_c})^M]_{jk} \mathscr{D}_k^{(-)} . \tag{76}$$

The Mth term in the infinite sum of eq. (76) represents the contributions of the $(M+1)$th return of the excited electron back to the reaction zone. The quantity $S_j = 2\pi\nu_j$ is just the classical action accumu-

lated during one revolution along a Kepler ellipse of maximal eccentricity ($l = 0$). With each return to the reaction zone the excited electron may be scattered into a different channel due to the presence of the residual core electrons. This scattering process is described by the scattering matrix χ_{cc}.

3.1.2. Atom in an external static field

If an atom is placed in a weak, static external field, a highly excited Rydberg electron may be strongly influenced at large distances from the ionic core. In this case Rydberg states of different n-manifolds are strongly mixed and the influence of the external field on the atom cannot be treated perturbatively [4].

Physically, we can distinguish three characteristic spatial regions as far as the dynamics of the excited Rydberg electron is concerned [102, 103]:

1. The atom–laser interaction [78] and electron correlation effects [9, 14] are concentrated in a *reaction zone*, which typically extends only a few Bohr radii around the atomic nucleus, i.e., $r \leq r_c \sim 1$.

2. In the surrounding *Coulomb zone*, i.e. for $r_c < r \ll a$, the electron is dominantly influenced by the $(1/r)$ Coulomb potential of the ionic core.

3. At sufficiently large distances from the ionic core, i.e. for $r \geq a$, the external potential $V_{ext}(\boldsymbol{x})$ becomes at least as important as the $(1/r)$ Coulomb potential. In general, the Hamiltonian which describes the dynamics of the excited electron in this *asymptotic zone* is not separable and the corresponding classical problem might even be nonintegrable.

This allows one to solve the Schrödinger equation (64) in two steps: In a first step we solve eq. (64) in the reaction and Coulomb zone with the methods of section 3.1.1. In a second step we solve eq. (64) in the Coulomb and asymptotic zone with the help of semiclassical methods and match both solutions inside the Coulomb zone.

For simplicity, we shall restrict the following discussion to the case of a single excitation channel. Thus, in the asymptotic part of the Coulomb zone the general solution of eq. (64) which is regular for $r \to 0$ is given by

$$F(\varepsilon, \boldsymbol{x}) \sim \sum_{l,m} Y_l^m(\theta, \varphi) \frac{1}{r} [-\varphi_l^{(+)}(\varepsilon, r) \mathrm{i}\pi \mathscr{D}_{lm}^{(-)} + \mathscr{F}_l^{(-)}(\varepsilon, r)^* \mathscr{A}_{lm}(\varepsilon)] \quad (1 \ll r \ll a), \tag{77}$$

in the notation of section 3.1.1 [compare with eq. (72)]. The radial solutions of the homogeneous part of eq. (64), $\mathscr{F}_l^{(-)}(\varepsilon, r)$, involve scattering matrix elements χ_l which describe elastic scattering of the valence electron inside the core region due to the presence of the residual electrons. For simplicity we assume this scattering to be spherically symmetric so that χ_l is independent of the magnetic quantum numbers m_l. Typically, this scattering process affects only low angular momentum states with $l < l_0$, which have a sufficiently large overlap with the ionic core. Thus we may write $\chi_l = 1 + f_l$ with the scattering amplitudes f_l being zero for $l > l_0$, approximately.

For the evaluation of $\mathscr{A}_{lm}(\varepsilon)$ we have to solve eq. (64) in the region $|\boldsymbol{x}| \geq r_0$ with the boundary condition

$$\psi_\varepsilon(\boldsymbol{x})|_{|\boldsymbol{x}|=r_0} = F(\varepsilon, \boldsymbol{x})_{|\boldsymbol{x}|=r_0} \quad (1 \ll r_0 \ll a). \tag{78}$$

The large extension of the classically accessible region implies large classical actions. Therefore this boundary value problem may be solved with the help of semiclassical methods. For this purpose we start from the part of $F(\varepsilon, \boldsymbol{x})$ which is proportional to $\varphi^{(+)}(\varepsilon, r)$, i.e. $\psi_{out}(\boldsymbol{x})$. For small angular momenta, $l, m \sim 1$, $\psi_{out}(\boldsymbol{x})$ involves a rapidly oscillating radial function and a slowly varying function of

θ and φ. For fixed value of the energy the rapidly oscillating radial part defines the two-dimensional Lagrangian manifold [95, 96]

$$L_0 = \{(r_0, \theta_0, \varphi_0, p_{r_0}, p_{\theta_0}, p_{\varphi_0}) \,|\, 0 < \theta_0 < \pi, 0 < \varphi_0 < 2\pi, p_{r_0} = \sqrt{2(\varepsilon + 1/r_0)}, p_{\theta_0} = p_{\varphi_0} = 0\} .$$

Propagating L_0 through phase space along the Hamiltonian flow generated by the classical Hamiltonian $H = \frac{1}{2}\boldsymbol{p}^2 - 1/r + V_{\text{ext}}(\boldsymbol{x})$ we obtain the three-dimensional Lagrangian manifold

$$L = \{(r, \theta, \varphi, p_r, p_\theta, p_\varphi)(\tau, \theta_0, \varphi_0) \,|\, 0 < \theta_0 < \pi, 0 < \varphi_0 < 2\pi, \tau \geq 0\} .$$

In the limit of large classical actions the solution of the boundary value problem is given by [95, 96]

$$\psi_\varepsilon(\boldsymbol{x}) = \sum_j \sqrt{J(0, \theta_{0j}, \varphi_{0j})/|J(\tau_j, \theta_{0j}, \varphi_{0j})|} \times \exp\{\mathrm{i}[S_\varepsilon(\tau_j, \theta_{0j}, \varphi_{0j}) - \mu_j^> \pi/2]\}\, \psi_{\text{out}}(r_0, \theta_{0j}, \varphi_{0j}) \quad (|\boldsymbol{x}| \geq r_0) , \tag{79}$$

asymptotically. The summation index j represents a sum over all projections of L onto the three-dimensional configuration space at point $\boldsymbol{x}$ and $S_\varepsilon(\tau_j, \theta_{0j}, \varphi_{0j})$ is the classical action along trajectory j which starts at point $(r_0, \theta_{0j}, \varphi_{0j})$ with $\tau = 0$ and reaches point $\boldsymbol{x}$ with $\tau = \tau_j$. The amplitudes of this asymptotic wave function are determined by the determinant of the local projection of the Lagrangian manifold L onto configuration space at point $\boldsymbol{x}$, i.e.,

$$J(\tau_j, \theta_{0j}, \varphi_{0j}) = \left.\frac{\mathrm{d}x \wedge \mathrm{d}y \wedge \mathrm{d}z}{\mathrm{d}\tau \wedge \mathrm{d}\theta_0 \wedge \mathrm{d}\varphi_0}\right|_{(\tau_j, \theta_{0j}, \varphi_{0j})} . \tag{80}$$

Its initial value, i.e. $J(0, \theta_{0j}, \varphi_{0j})$, is determined by L_0. $\mu_j^>$ is the Maslov index [95, 96] of trajectory j outside the Coulomb zone. The unknown amplitudes $\mathscr{A}_{lm}(\varepsilon)$ of eq. (77) are determined by the boundary condition (78), which implies

$$\mathscr{A}_{lm}(\varepsilon) = \int_0^{2\pi} \mathrm{d}\varphi \int_0^{\pi} \mathrm{d}\theta \sin\theta\, Y_l^m(\theta, \varphi)^* (-1)^l \sum_j \sqrt{J(0, \theta_{0j}, \varphi_{0j})/|J(\tau_j, \theta_{0j}, \varphi_{0j})|} \times \exp\{\mathrm{i}[2w_\varepsilon(r_1, r_0) + S_\varepsilon(\tau_j, \theta_{0j}, \varphi_{0j}) - (\mu_j^> + 3)\pi/2]\} \times \sum_{l'm'} Y_{l'}^{m'}(\theta_{0j}, \varphi_{0j})(-1)^{l'} [2\mathrm{i}\pi \mathscr{D}_{l'm'}^{(-)} + (1 + f_{l'})\mathscr{A}_{l'm'}(\varepsilon)] , \tag{81}$$

with $r(\tau_j, \theta_{0j}, \varphi_{0j}) = r_0$, $\tau_j > 0$ and $p_r(\tau_j, \theta_{0j}, \varphi_{0j}) < 0$.

In general, eq. (81) can only be solved approximately. A special case arises in the absence of an external field, where $\mathscr{A}_{lm}(\varepsilon)$ may be evaluated exactly. The rotational symmetry of the Coulomb problem implies that the action $S_\varepsilon(\tau_j, \theta_{0j}, \varphi_{0j})$ is independent of the final angles θ and φ. Below threshold therefore the contributions of *all bound trajectories*, which start from the nucleus with a pure radial momentum and return again to $|\boldsymbol{x}| = r_0$, interfere *constructively*. Taking into account that $S_\varepsilon(\tau_j, \theta_{0j}, \varphi_{0j}) + 2w_\varepsilon(r_1, r_0) = 2\pi\nu$ with $\varepsilon = -1/(2\nu^2) < 0$, we obtain

$$\mathscr{A}_{lm}(\varepsilon) = \mathrm{e}^{\mathrm{i}(2\pi\nu - 4\pi/2)} [2\mathrm{i}\pi \mathscr{D}_{lm}^{(-)} + \chi_l \mathscr{A}_{lm}(\varepsilon)] \quad (\varepsilon < 0) . \tag{82}$$

Inserting eq. (82) into eqs. (77) and (65) gives the one-channel approximation of the classical path representation as given in eq. (76).

In a static external field the rotational symmetry of the Coulomb problem is broken. In general, this implies that $\exp[\mathrm{i}S_\varepsilon(\tau_j, \theta_{0j}, \varphi_{0j})]$ is a rapidly oscillating function of the final angles θ and φ. In this case, the dominant contributions to $\mathscr{A}_{lm}(\varepsilon)$ come from points of stationary phase, where $p_\theta = p_\varphi = 0$ and the trajectories return to the Coulomb zone with a pure radial momentum. Solving eq. (81) iteratively in the stationary phase approximation yields $\mathscr{A}_{lm}(\varepsilon)$ as a sum of contributions of repeated returns of all *isolated, closed trajectories*, which start from the nucleus. The first iteration of eq. (81) gives for small angular momenta $l, m \sim 1$,

$$\mathscr{A}_{lm}(\varepsilon) = \sum_j Y_l^m(\theta_j, \varphi_j)^*(-1)^l \sqrt{\sin\theta_j \sin\theta_{0j}}\, \sqrt{(2\pi)^2 \Big/ \left|\frac{\mathrm{d}p_\theta \wedge \mathrm{d}p_\varphi}{\mathrm{d}\theta_0 \wedge \mathrm{d}\varphi_0}\right|_{(\tau,\theta_{0j},\varphi_{0j})}}$$
$$\times \exp\left\{\mathrm{i}\left[S_j(\varepsilon) - \mu_j\pi/2 + \mathrm{sgn}\left(\frac{\partial(p_\theta, p_\varphi)}{\partial(\theta,\varphi)}\right)\pi/4\right]\right\}$$
$$\times \sum_{l'm'} Y_{l'}^{m'}(\theta_{0j}, \varphi_{0j})(-1)^{l'} 2\mathrm{i}\pi \mathscr{D}^{(-)}_{l'm'} + \mathrm{O}(\lambda^{-2})\,. \tag{83}$$

The leading contribution of a closed orbit to $\mathscr{A}_{lm}(\varepsilon)$ is therefore of order λ^{-1} with λ denoting the order of magnitude of the classical actions, $S_j(\varepsilon)$, along the closed orbits. This reflects the fact that only classical trajectories, which return to the Coulomb zone in a small neighborhood of a closed orbit within a solid angle of order $(\lambda^{-1/2})^2$, significantly contribute to $\mathscr{A}_{lm}(\varepsilon)$. The sum over j includes all closed orbits which start from the Coulomb zone with a pure radial momentum. The Maslov indices of the closed orbits are denoted μ_j. The Jacobian matrix $\partial(p_\theta, p_\varphi)/\partial(\theta,\varphi)$ is evaluated at $r = r_0$ when the closed orbit leaves the Coulomb zone again. This stationary phase evaluation is valid as long as all closed orbits are isolated and stationary phase contributions are well separated. The second iteration of eq. (81) gives the contributions of the second return of the classical trajectories to the Coulomb zone. Contributions from closed orbits which have not been scattered during their first return to the reaction zone are of order λ^{-1}. In the approximation that only a few of the scattering amplitudes f_l are not equal to zero, contributions from scattered orbits are of order $\mathrm{O}(\lambda^{-2})$. Therefore, in the limit of large classical actions they may be neglected. With this approximation we finally find for the two-photon transition amplitude

$$T_{\mathrm{fi}}(\varepsilon) = T_{\mathrm{fi}}^{(\mathrm{s})} + 2\mathrm{i}\pi \sum_m \sum_{jM_j} d_m^{(+)}(\theta_j, \varphi_j) \sqrt{\sin\theta_j \sin\theta_{0j}}\, \sqrt{(2\pi)^2 \Big/ \left|\frac{\mathrm{d}p_\theta \wedge \mathrm{d}p_\varphi}{\mathrm{d}\theta_0 \wedge \mathrm{d}\varphi_0}\right|^{(M_j)}_{(\tau_j,\theta_{0j},\varphi_{0j})}}$$
$$\times \exp\left\{\mathrm{i}\left[M_j[S_j(\varepsilon) - \mu_j\pi/2] + \mathrm{sgn}\left(\frac{\partial(p_\theta, p_\varphi)}{\partial(\theta,\varphi)}\right)\pi/4\right]\right\} d_m^{(-)}(\theta_{0j}, \varphi_{0j})\,. \tag{84}$$

The M_jth term in this classical path representation represents the contribution of the M_jth return of the isolated, closed orbit j to the Coulomb zone. The amplitude of this contribution is determined by the corresponding cross section

$$\frac{\mathrm{d}p_Q^{(M_j)}}{\mathrm{d}\Omega_0} = (\sin\theta_j \sin\theta_{0j})^{-1} \left|\frac{\mathrm{d}p_\theta \wedge \mathrm{d}p_\varphi}{\mathrm{d}\theta_0 \wedge \mathrm{d}\varphi_0}\right|^{(M_j)}_{(\tau_j,\theta_{0j},\varphi_{0j})}.$$

In the approximation of eq. (84) effects of a nonhydrogenic core manifest themselves only in the initial

excitation and final recombination processes, which are described by the photoionization and recombination dipole matrix elements

$$d_m^{(-)}(\theta_{j0}, \varphi_{j0}) = \sum_l \mathscr{D}_{lm}^{(-)} Y_l^m(\theta_{j0}, \varphi_{j0})(-1)^l , \qquad d_m^{(+)}(\theta_j, \varphi_j) = \sum_l \mathscr{D}_{lm}^{(+)} Y_l^m(\theta_j, \varphi_j)^*(-1)^l .$$

We conclude by pointing out that there exists already an extensive literature on the theoretical description of wave packet propagation, both in molecular and nuclear physics [104]. An early systematic approach to the time evolution of wave packets has been developed by Heller and coworkers [105–117]. It is essentially numerically oriented and is based on representing an approximate solution of the time dependent Schrödinger equation as a sum of Gaussian wave packets which are propagated along the classical trajectories of the system. The parameters of these Gaussians are determined by expanding the potential up to quadratic terms about the instantaneous centers of the wave packets. This method has been applied to investigate a variety of problems in molecular physics, for example photodissociation [118, 119], photofragmentation [120, 121], vibrational Raman scattering [122–125] and gas–surface scattering [126–128]. However, so far applications of this method to the description of molecular laser excitation processes have focused mainly on excitation processes which involve long laser pulses and may therefore be characterized by a time independent photoabsorption cross section. In this context the time dependent Gaussian wave packets have been used as a calculational tool to evaluate the molecular dipole autocorrelation function, whose Fourier transform determines the laser excitation rate [129].

3.2. Minimum-uncertainty energy eigenstates

Since Schrödinger's discussion of the coherent states of the harmonic oscillator there have been various attempts to construct electronic wave packets which are localized on Kepler ellipses with minimum quantum fluctuations [49–56]. Such ideal Kepler wave packets are of particular interest, because they provide a natural bridge between quantum mechanics and the classical concept of the trajectory of an electron which moves in a Coulomb potential. Recently, it has been shown how hydrogenic energy eigenstates which are localized along Kepler ellipses with minimum quantum fluctuations, can be excited by a laser pulse [45, 56, 57]. A coherent superposition of a large number of such minimum uncertainty energy eigenstates with different energies would represent an ideal Kepler wave packet [45, 56]. These states and wave packets constructed with these states might have interesting applications.

Minimum-uncertainty energy eigenstates have been introduced recently by Delande and Gay [57] and Nauenberg [56]. These states are coherent superpositions of hydrogenic energy eigenstates with different values of the angular momentum. Their probability distributions are stationary and are localized along Kepler ellipses. The quantum fluctuations of these states are as small as possible compatible with Heisenberg's uncertainty relations. Coherent laser excitation of these states would generate an ideal Kepler wave packet which moves along a Kepler orbit for all times [45, 56]. Experimentally, such minimum-uncertainty states have been prepared with the help of microwave fields [46, 47] and recently also with the help of crossed electric and magnetic fields [48].

In the construction of these states the SO(4) symmetry of the Coulomb problem is of central importance [45, 56, 57]. From the angular momentum $\boldsymbol{l} = \boldsymbol{x} \times \boldsymbol{p}$ and the Runge–Lenz–Pauli vector

$$\boldsymbol{a} = (-2\varepsilon)^{-1/2}[\tfrac{1}{2}(\boldsymbol{p} \times \boldsymbol{l} - \boldsymbol{l} \times \boldsymbol{p}) - \boldsymbol{x}/r] \quad (\varepsilon < 0) , \tag{85}$$

which both commute with the nonrelativistic hydrogenic Hamiltonian, we may construct two independent angular momentum operators

$$\boldsymbol{j}_{1,2} = \tfrac{1}{2}(\boldsymbol{l} \mp \boldsymbol{a}) . \tag{86}$$

From eqs. (85) and (86) we find $\boldsymbol{l}\cdot\boldsymbol{a} = \boldsymbol{a}\cdot\boldsymbol{l} = 0$ and $\boldsymbol{j}_1^2 = \boldsymbol{j}_2^2 = \frac{1}{4}(\boldsymbol{l}^2 + \boldsymbol{a}^2) = \frac{1}{4}(n^2 - 1)$. All hydrogenic energy eigenstates with energy $\varepsilon = -1/(2n^2) < 0$ may therefore be chosen as eigenstates of $\boldsymbol{j}_1^2$ and $\boldsymbol{j}_2^2$ with $j_1 = j_2 = (n-1)/2$. An angular momentum eigenstate $|j\boldsymbol{u}\rangle$ with maximum (minimum) eigenvalue $m_j = j$ ($m_j = -j$) along the quantization axis $\boldsymbol{u}$ ($\boldsymbol{u}^2 = 1$) implies minimum quantum fluctuations of the angular momentum around its mean value $\langle \boldsymbol{j} \rangle = \boldsymbol{u} m_j$, i.e., $\Delta \boldsymbol{j} = (\langle \boldsymbol{j}^2 \rangle - \langle \boldsymbol{j} \rangle^2)^{1/2} = \sqrt{j}$. The hydrogenic energy eigenstate [45]

$$|n\alpha\rangle = |j_1 \boldsymbol{u}_1\rangle \otimes |j_2 \boldsymbol{u}_2\rangle \tag{87}$$

with $m_{j_1} = m_{j_2} = (n-1)/2$, for example, therefore implies minimum fluctuations of the angular momentum and the Runge–Lenz–Pauli vector around their mean values. The quantity $(\Delta \boldsymbol{l})^2 + (\Delta \boldsymbol{a})^2 = 2(\Delta \boldsymbol{j}_1)^2 + 2(\Delta \boldsymbol{j}_2)^2 = 2(n-1)$ is therefore as small as possible compatible with Heisenberg's uncertainty relations. Choosing the z-axis as the first and the x-axis as the second bisector of $(\boldsymbol{u}_1, \boldsymbol{u}_2)$ and denoting $2\alpha = \angle(\boldsymbol{u}_1, \boldsymbol{u}_2)$, the mean values of the angular momentum and the Runge–Lenz–Pauli vector in the state of eq. (87) are given by

$$\langle l_x \rangle = \langle l_y \rangle = \langle a_y \rangle = \langle a_z \rangle = 0 , \qquad \langle a_x \rangle = (n-1)\sin\alpha , \qquad \langle l_z \rangle = (n-1)\cos\alpha . \tag{88}$$

Classically these mean values define a Kepler ellipse located in the x–y-plane with major axis along the x-axis and eccentricity $e = \sin\alpha$. A special case of these elliptic states are the circular states with $\alpha = 0$ ($l = m = n-1$), which are localized on a circle in the x–y-plane. Linear superpositions of hydrogenic eigenstates $|n\alpha\rangle$ with different energies would represent an ideal Kepler wave packet [56].

A method for preparing these elliptic states, $|n\alpha\rangle$, by laser excitation in weak crossed electric and magnetic fields has been proposed recently by Delande and Gay [57]. Neglecting diamagnetism, the nonrelativistic hydrogenic Hamiltonian in weak crossed electric and magnetic fields is given by

$$H = p^2/2 - 1/r + \tfrac{1}{2}Bl_z + Fx , \tag{89}$$

with the magnetic and electric field strengths B and F in atomic units. (The atomic units of the magnetic and electric field strength are $B_0 = 2.35 \times 10^5$ T and $F_0 = 5.14 \times 10^{11}$ V m^{-1}.) If the external fields are so weak that n-mixing is negligible, we may perform the Pauli replacement $x = -\frac{3}{2}na_x$ within a particular n-shell and the interaction Hamiltonian reduces to

$$W_n = \tfrac{1}{2}Bl_z - \tfrac{3}{2}nFa_x = \sqrt{(B/2)^2 + \omega_S^2}\ \boldsymbol{\lambda}\cdot\boldsymbol{u}_2 , \tag{90}$$

with $\boldsymbol{u}_2 = (\sin\alpha, 0, \cos\alpha)$, $\tan\alpha = 2\omega_S/B$ and the Stark frequency $\omega_S = -\frac{3}{2}nF$. From the quantum mechanical commutation relations between the components of $\boldsymbol{l}$ and $\boldsymbol{a}$ we find that $\boldsymbol{\lambda} = (a_x, a_y, l_z)$ is an angular momentum operator. The eigenstates of the Hamiltonian H can therefore be chosen as eigenstates of $\boldsymbol{\lambda}^2$ and $\boldsymbol{\lambda}\cdot\boldsymbol{u}_2$ with eigenvalues $\lambda(\lambda+1)$ and k ($|k| \le \lambda \le n-1$, $-(n-1) \le k \le n-1$),

respectively [130, 131]. The corresponding energy eigenvalues are

$$E_n = -1/(2n^2) + k\sqrt{(B/2)^2 + \omega_S^2}\,. \tag{91}$$

From eq. (87) we find

$$\boldsymbol{\lambda}^2|n\alpha\rangle = \lambda(\lambda+1)|n\alpha\rangle\,, \tag{92}$$

$$\boldsymbol{\lambda}\cdot\boldsymbol{u}_2|n\alpha\rangle = (n-1)|n\alpha\rangle\,, \tag{93}$$

with $\lambda = n-1$ so that the highest energy eigenstate of the Hamiltonian of eq. (89) is the minimum-uncertainty state $|n\alpha\rangle$. (A similar argument applies for the lowest energy eigenstate.)

Thus, a minimum-uncertainty energy eigenstate may be excited in the following way: In a first step a laser pulse excites the uppermost energy eigenstate of a particular hydrogenic n-manifold in the Stark limit, $\omega_S \gg B/2$, so that the elliptic state $|n\alpha = \pi/2\rangle$ is prepared. This elliptic state of maximal eccentricity has a large overlap with any energetically low lying bound state and its laser-induced excitation is therefore very effective. In a second step the electric field is turned off and a weak magnetic field is turned on until a definite value α_0 is reached. If both fields are changed adiabatically, i.e. slowly in comparison with $[(B/2)^2 + \omega_S^2]^{-1/2}$, this procedure prepares the minimum-uncertainty state $|n\alpha_0\rangle$. With this method Hare et al. [48] have recently excited circular Rydberg states.

4. Dynamics of radial Rydberg wave packets

In this chapter we apply the methods developed in chapter 3 to discuss three problems of wave packet dynamics. As a first example we consider wave packets in many-electron atoms. The second example deals with one-photon resonant two-photon excitation close to threshold by a long and intense laser pulse. Finally, results are presented for wave packets in the presence of a static electric and magnetic field.

4.1. Electron correlation effects

In order to study the influence of electron correlation effects on the dynamics of a radial electronic wave packet we consider the simple case of laser excitation of an atom whose Rydberg and continuum states close to the photoionization threshold can be described approximately in a two-channel approximation as schematically shown in fig. 13. Both ionization thresholds correspond to excited states of the positively charged ionic core. Due to electron correlations both excited channels are coupled. This coupling is localized inside a reaction zone, which typically extends only a few Bohr radii around the atomic nucleus, and may be characterized by the 2×2 scattering matrix [9]

$$\chi = (1+\tau)^{-1}\begin{pmatrix} (1-\tau)\,e^{2i\pi\alpha} & 2i\sqrt{\tau}\,e^{i\pi(\alpha+\delta)} \\ 2i\sqrt{\tau}\,e^{i\pi(\alpha+\delta)} & (1-\tau)\,e^{2i\pi\delta} \end{pmatrix}. \tag{94}$$

Above both thresholds χ describes the inelastic electron–ion scattering due to the residual core electrons inside the finite reaction zone. It is a smooth function of energy across both thresholds. The

configuration interaction between both channels is characterized by the channel mixing parameter τ $(0<\tau<\infty)$, $\pi\alpha$ and $\pi\delta$ are continuum phase shifts.

If many Rydberg states close to one of the photoionization thresholds are excited coherently, for example by a short laser pulse, a radial Rydberg wave packet is generated, part of which returns again to the reaction zone, where it may exchange energy with the ionic core [18]. Therefore, probing this wave packet with a second short laser pulse, which induces, for example, a transition to an energetically low lying bound state $|f\rangle$, yields information about the electron correlation induced coupling between both fragmentation channels.

(i) *Autoionizing region.* For energies $I_1 > \varepsilon \geq I_2 = 0$ only channel 1 is closed and the classical path representation of the two-photon transition amplitude as given in eq. (76) reduces to

$$T_{fi}(\varepsilon) = T_{fi}^{(s)} + 2i\pi \sum_{M=0}^{\infty} \mathscr{D}_1^{(+)} e^{2i\pi\nu_1} (\chi_{11} e^{2i\pi\nu_1})^M \mathscr{D}_1^{(-)} . \tag{95}$$

The infinite sum describes the contributions from repeated returns of the excited electron back to the reaction zone. The scattering matrix element χ_{11} describes scattering of the excited electron within the closed-channel subspace.

The dashed curve of fig. 7 shows the two-photon Raman transition probability as evaluated from eqs. (95) and (37). Autoionizing Rydberg states around $\bar{\nu}_1 = 85$ are coherently excited in channel 1 by a short laser pulse at time t_a and are probed with a second pulse after a time delay $\Delta t = t_b - t_a$. Both laser pulses are assumed to have Gaussian pulse envelopes with the same pulse duration. The recombination peaks correspond to repeated returns of the excited electron to the reaction zone. Because of inelastic electron scattering inside the reaction zone we have $|\chi_{11}| < 1$. This leads to a decrease of the recombination peaks in comparison with the corresponding results in the absence of autoionization, which are shown by the solid curve of fig. 7 [18].

(ii) *Bound state region.* For energies $\varepsilon < 0$ both excited channels are closed and the first few terms of the classical path representation of the two-photon transition amplitude reduce to

$$\begin{aligned} T_{fi}(\varepsilon) = T_{fi}^{(s)} + 2i\pi[& \mathscr{D}_1^{(+)} e^{2i\pi\nu_1} \mathscr{D}_1^{(-)} + \mathscr{D}_2^{(+)} e^{2i\pi\nu_2} \mathscr{D}_2^{(-)} \\ & + \mathscr{D}_1^{(+)} e^{2i\pi\nu_1} \chi_{11} e^{2i\pi\nu_1} \mathscr{D}_1^{(-)} + \mathscr{D}_2^{(+)} e^{2i\pi\nu_2} \chi_{22} e^{2i\pi\nu_2} \mathscr{D}_2^{(-)} \\ & + \mathscr{D}_1^{(+)} e^{2i\pi\nu_1} \chi_{12} e^{2i\pi\nu_2} \mathscr{D}_2^{(-)} + \mathscr{D}_2^{(+)} e^{2i\pi\nu_2} \chi_{21} e^{2i\pi\nu_1} \mathscr{D}_1^{(-)} + \cdots] \quad (\varepsilon < 0) . \end{aligned} \tag{96}$$

The classical action $S_j = 2\pi\nu_j$ corresponds to one revolution of the excited electron in channel j along a Kepler ellipse of maximal eccentricity. The 2×2 scattering matrix χ describes the electron scattering between both excited channels, which takes place inside the reaction zone.

Figure 14 shows the two-photon Raman transition probability as evaluated from eqs. (96) and (37). A first, short laser pulse excites Rydberg states around $\bar{\nu}_2 = 89$. Because of the configuration-interaction-induced coupling between both excited channels, two Rydberg wave packets with different mean classical orbit times are generated. Their time evolution is probed with a second short laser pulse after a time delay Δt. Each recombination peak of fig. 14 corresponds to the return of one of the wave packets to the reaction zone. The recombination peak at time $\Delta t \approx T_1 + T_2$ is due to inelastic scattering of one of the wave packets during the first return to the reaction zone and vanishes in the absence of channel coupling. It is described by the 6th and 7th terms on the r.h.s. of eq. (96). If both wave packets return to the reaction zone simultaneously, they interfere. In fig. 14 complete destructive interference between both wave packets occurs at time $\Delta t \approx 3T_1 \approx 2T_2$ and the corresponding recombination peak vanishes.

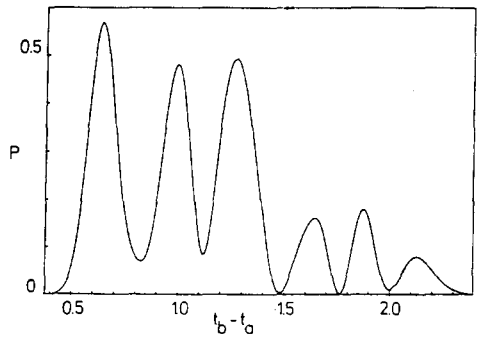

Fig. 14. Two-photon Raman transition probability R (in arbitrary units) versus time delay between both laser pulses in units of the mean classical orbit time $T_2 = 107$ ps, with $\bar{\varepsilon} = \varepsilon_i + \omega_a = \varepsilon_f + \omega_b$, pulse duration $\tau_p = 14$ ps, mixing parameter $\tau = 0.02$, Fano parameter $q = -7$ and $I_1 = 0.63$ meV (corresponding to $\bar{\nu}_1 = 76$, $T_1 = T_2/1.6$).

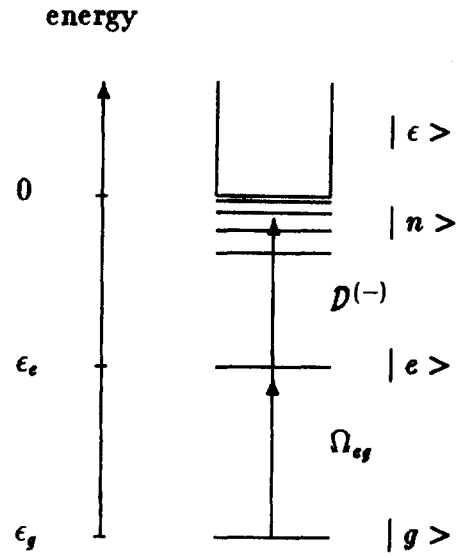

Fig. 15. Schematic representation of the laser excitation process.

4.2. *Resonant two-photon excitation*

Here we generalize the discussion of depletion wave packets (subsection 2.2.3) to two bound states which are resonantly coupled (fig. 15 [32]). A first long and intense laser pulse induces a resonant transition from an initial state $|g\rangle$ to an excited state $|e\rangle$. A second laser pulse, which overlaps with the first one, subsequently excites the atom to Rydberg and continuum states close to the photoionization threshold. Both laser pulses are assumed to have rectangular pulse shapes and are turned on instantaneously at $t = 0$.

The dynamics of this excitation process is determined by four main parameters: the Rabi frequency of the transition $|g\rangle \rightarrow |e\rangle$, $\Omega_{eg} = 2\langle e|\boldsymbol{\mu}\cdot\boldsymbol{\varepsilon}_1|g\rangle\mathscr{E}_1$; the detuning from resonance, $\Delta = \varepsilon_g + \omega_1 - \varepsilon_e$; the ionization rate from the excited state $|e\rangle$, Γ; and the level spacing between adjacent Rydberg states, $\Delta\varepsilon_n = (n-\alpha)^{-3}$.

In the rotating wave approximation the initial-state probability amplitude of the atom at time t is given by [32]

$$a_g(t) = \frac{1}{2\pi}\int_{-\infty+i0}^{\infty+i0} d\varepsilon\, e^{-i(\varepsilon-\omega_1-\omega_2)t}\{i[\varepsilon - H_{bb} - \Sigma_{bb}(\varepsilon)]^{-1}\}_{gg}\,. \tag{97}$$

The Hamiltonian matrix

$$H_{bb} = \begin{pmatrix} \varepsilon_g + \omega_1 + \omega_2 & \frac{1}{2}\Omega_{eg} \\ \frac{1}{2}\Omega_{eg} & \varepsilon_e + \omega_2 \end{pmatrix} \tag{98}$$

describes the field-induced coupling between both bound states. The self-energy matrix of the bound states is given by

$$\Sigma_{\mathrm{bb}}(\varepsilon)=\begin{pmatrix}0 & 0\\ 0 & 1\end{pmatrix}\times\begin{cases}\delta\omega-\mathrm{i}\Gamma/2\equiv\Sigma_{\mathrm{bb}}^{(\mathrm{s})} & (\varepsilon\geq 0)\,,\\ \delta\omega-\mathrm{i}\Gamma/2+2\pi\mathrm{i}\mathscr{D}^{(+)}\,\mathrm{e}^{2\mathrm{i}\pi\nu}(1-\chi\,\mathrm{e}^{2\mathrm{i}\pi\nu})^{-1}\mathscr{D}^{(-)}|\mathscr{E}_2|^2 & (\varepsilon=-\tfrac{1}{2}\nu^{-2}<0)\,,\end{cases} \tag{99}$$

and describes effects of the laser-induced coupling between the excited state $|\mathrm{e}\rangle$ and the Rydberg and continuum states close to threshold. The quadratic Stark shift between the excited state $|\mathrm{e}\rangle$ and the Rydberg and continuum states is denoted $\delta\omega$ and includes the ponderomotive shift of the ionization threshold. Both the quadratic Stark shift and the ionization rate Γ are slowly varying functions of energy across threshold. The scattering matrix element $\chi=\mathrm{e}^{2\mathrm{i}\pi\alpha}$ describes elastic electron–ion scattering inside the reaction zone. The photoionization and recombination dipole matrix elements $\mathscr{D}^{(-)}$ and $\mathscr{D}^{(+)}$ characterize the laser-induced coupling between state $|\mathrm{e}\rangle$ and the Rydberg and continuum states.

With the methods of subsection 2.2.3 we may derive a classical path representation for the initial-state probability amplitude [32]

$$\begin{aligned}a_{\mathrm{g}}(t)=\tfrac{1}{2\pi}&\int_{-\infty+\mathrm{i}0}^{\infty+\mathrm{i}0}\mathrm{d}\varepsilon\,\mathrm{e}^{-\mathrm{i}(\varepsilon-\omega_1-\omega_2)t}[\mathrm{i}(\varepsilon-H_{\mathrm{bb}}-\Sigma_{\mathrm{bb}}^{(\mathrm{s})})^{-1}]_{\mathrm{gg}}\\ &+\sum_{M=0}^{\infty}\int_{-\infty}^{0}\mathrm{d}\varepsilon\,\mathrm{e}^{-\mathrm{i}(\varepsilon-\omega_1-\omega_2)t}[\mathrm{i}(\varepsilon-H_{\mathrm{bb}}-\Sigma_{\mathrm{bb}}^{(\mathrm{s})})^{-1}]_{\mathrm{ge}}\mathscr{D}^{(+)}\\ &\times\mathrm{e}^{2\mathrm{i}\pi\nu}(\tilde{\chi}(\varepsilon)\,\mathrm{e}^{2\mathrm{i}\pi\nu})^{M}\mathscr{D}^{(-)}[\mathrm{i}(\varepsilon-H_{\mathrm{bb}}-\Sigma_{\mathrm{bb}}^{(\mathrm{s})})^{-1}]_{\mathrm{eg}}|\mathscr{E}_2|^2\,,\end{aligned} \tag{100}$$

with the infinite sum on the r.h.s. representing contributions from repeated returns of the excited Rydberg electron back to the reaction zone. The scattering matrix element

$$\tilde{\chi}(\varepsilon)=\chi+2\pi\mathscr{D}^{(-)}[\mathrm{i}(\varepsilon-H_{\mathrm{bb}}-\Sigma_{\mathrm{bb}}^{(\mathrm{s})})^{-1}]_{\mathrm{ee}}\mathscr{D}^{(+)}|\mathscr{E}_2|^2 \tag{101}$$

describes electron–ion scattering between the excited Rydberg electron and the ionic core inside the reaction zone in the presence of the laser field.

If the initial state $|\mathrm{g}\rangle$ is depleted on a time scale short in comparison with the mean classical orbit time of the excited Rydberg states, a radial electronic wave packet is generated [30, 32]. In the case of long laser pulses such a short depletion time is achieved by using sufficiently high laser intensities. If the first laser pulse is tuned on resonance, i.e. $\Delta=0$, and is so intense that $1/|\Omega_{\mathrm{eg}}|\ll 1/\Gamma\ll T_{\bar{\varepsilon}}=2\pi(-2\bar{\varepsilon})^{-3/2}$ with $\bar{\varepsilon}=\varepsilon_{\mathrm{e}}+\omega_2$, the energies of the strongly coupled bound states are split due to the AC Stark effect and two radial Rydberg wave packets are generated with mean energies $\bar{\varepsilon}_1=\bar{\varepsilon}-\frac{1}{2}\Omega_{\mathrm{eg}}$ and $\bar{\varepsilon}_2=\bar{\varepsilon}+\frac{1}{2}\Omega_{\mathrm{eg}}$.

Figure 16 shows the initial-state probability as a function of the interaction time as evaluated from eq. (100). Rydberg and continuum states around $\bar{\nu}=250$ are excited by an intense laser pulse. For times short in comparison with both classical orbit times, the generated radial wave packets have not been reflected at the outer turning points of their orbits and behave like in a typical one-photon resonant two-photon ionization process. Therefore, the initial-state probability shows Rabi oscillations originating from the strong coupling between $|\mathrm{e}\rangle$ and $|\mathrm{g}\rangle$ which decay exponentially on a time scale of the order of $1/\Gamma$ because of ionization. This short-time behavior is described by the first term of the

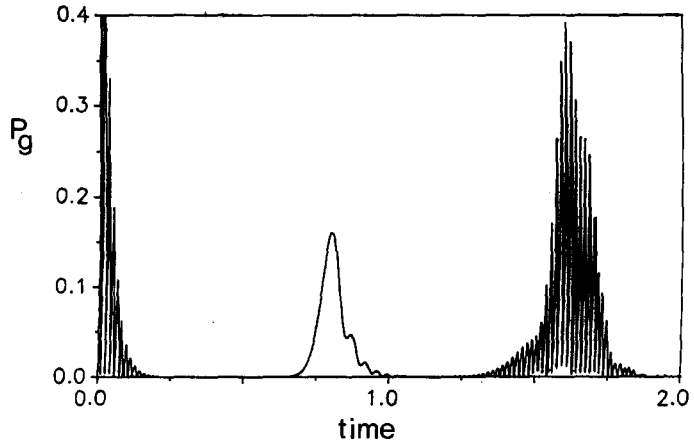

Fig. 16. Initial-state probability P_g as a function of interaction time in units of the mean classical orbit time $T_{\bar{\varepsilon}} = 2.37$ ns for $1/|\Omega_{eg}| = 6.0$ ps, $1/\Gamma = 35$ ps, $\Delta = 0$ and $\alpha = 0$.

classical path representation of eq. (100). Eventually, the wave packets are reflected at the outer turning points of their orbits and return again to the reaction zone, where the laser field may induce transitions to one of the dressed states of the strongly coupled states $|e\rangle$ and $|g\rangle$. This recombination process leads to an increase of the initial-state probability. The first recombination peak in fig. 16 corresponds to the first return of the faster wave packet to the reaction zone. For the parameters shown in fig. 16 we have $3T_{\bar{\varepsilon}-(1/2)\Omega_{eg}} = 2T_{\bar{\varepsilon}+(1/2)\Omega_{eg}}$, so that the faster wave packet overlaps with the slower one inside the reaction zone at time $t \approx 3T_{\bar{\varepsilon}-(1/2)\Omega_{eg}}$. The interference between both wave packets leads to rapid oscillations of the initial-state probability with frequency Ω_{eg}.

4.3. *External static fields*

In this section we study the influence of an external static electric or magnetic field on the dynamics of an initially prepared radial Rydberg wave packet [34, 36].

4.3.1. *Static electric field*

If an atom is placed in a weak, static electric field, $\boldsymbol{F} = F\boldsymbol{e}_z$, the dynamics of a highly excited Rydberg electron is significantly modified at large distances from the positively charged ionic core [4, 102, 103, 132–145]. The characteristic distance, $a = F^{-1/2}$, at which the external potential $V_{ext}(\boldsymbol{x}) = -\boldsymbol{\mu} \cdot \boldsymbol{e}_z F$ becomes equal to the $(1/r)$ Coulomb potential of the ionic core, measures the extension of the Coulomb zone. (The atomic unit of electric field strength is given by $F_0 = 5.14 \times 10^{11}$ V m^{-1}.) Therefore, in the case of weak electric fields with typical field strengths of the order of a few kV/cm the classically assessible region of configuration space is large. This implies large classical actions and atomic transition amplitudes may be evaluated with the semiclassical methods described in subsection 3.1.2. In particular, we may derive classical path representations in which the transition amplitudes are expressed as a sum of contributions of all isolated, closed orbits of the excited electron which start from the nucleus.

A characteristic feature of the classical dynamics of a highly excited Rydberg electron under the influence of a Coulomb field and an external static electric field is the appearance of one isolated, periodic orbit for energies above the zero-field photoionization threshold [132–145]. The Hamiltonian, which describes the motion of the excited electron in the Coulomb and asymptotic zone, is axially

symmetric around the electric field axis. The periodic orbit starts from the nucleus and extends along this symmetry axis in the direction of the applied field. Because of the separability of the classical Hamiltonian in parabolic coordinates, the classical properties of this orbit can easily be determined analytically [34, 100]. Its action is given by

$$S(\varepsilon) = F^{-1/4}(1+\tilde{\varepsilon}^2)^{-1/4} \cdot \tfrac{8}{3}\{(1+\tilde{\varepsilon}^2)^{1/2}[(1+\tilde{\varepsilon}^2)^{1/2} - \tilde{\varepsilon}]K(\kappa) + 2\tilde{\varepsilon}(1+\tilde{\varepsilon}^2)^{1/2}E(\kappa)\}\,, \tag{102}$$

with $\kappa = \frac{1}{2}[\tilde{\varepsilon} + (1+\tilde{\varepsilon}^2)^{1/2}](1+\tilde{\varepsilon}^2)^{-1/2}$, the scaled energy $\tilde{\varepsilon} = \varepsilon/(2\sqrt{F})$ and the complete elliptic integrals of the first and second kind $K(\kappa)$ and $E(\kappa)$ as defined in ref. [86]. The Maslov index of this periodic orbit is given by $\mu = 2$ and its instability properties are characterized by the cross section

$$\left(\frac{\mathrm{d}p_\Omega}{\mathrm{d}\Omega_0}\right)^{(M)} = (\sin\theta_0 \sin\theta)^{-1}\left|\frac{\mathrm{d}p_\theta \wedge \mathrm{d}p_\varphi}{\mathrm{d}\theta_0 \wedge \mathrm{d}\varphi_0}\right|_{r_0}^{(M)} = [\sinh(Mu)/\sqrt{2\varepsilon}]^2\,. \tag{103}$$

The energy dependence of the stability exponent

$$u = 2\sqrt{\tilde{\varepsilon}}(1+\tilde{\varepsilon}^2)^{-1/4}K(\kappa) \quad (\varepsilon \geq 0) \tag{104}$$

is shown in fig. 17. Inserting eqs. (102)–(104) into eq. (84) we obtain the classical path representation for the two-photon transition amplitude [34, 100]

$$T_{\mathrm{fi}}(\varepsilon) = T_{\mathrm{fi}}^{(\mathrm{s})} + \delta_{m0} d_m^{(+)}(0,0)\, 2\mathrm{i}\pi \sum_{M=1}^{\infty} \frac{2\pi\sqrt{2\varepsilon}}{\sinh(Mu)}\, \mathrm{e}^{\mathrm{i}\{M[S(\varepsilon)-2\pi/2]-2\pi/4\}} d_M^{(-)}(0,0) \quad (\varepsilon \geq 0)\,. \tag{105}$$

The contributions of the repeated returns of the isolated, closed orbit to the reaction zone are of order $(\lambda^{-1/2})^2$ with $\lambda = \sqrt{a}$ denoting the order of magnitude of the classical action. It has been shown in subsection 3.1.2 that in the limit of large classical actions effects of a nonhydrogenic core are only

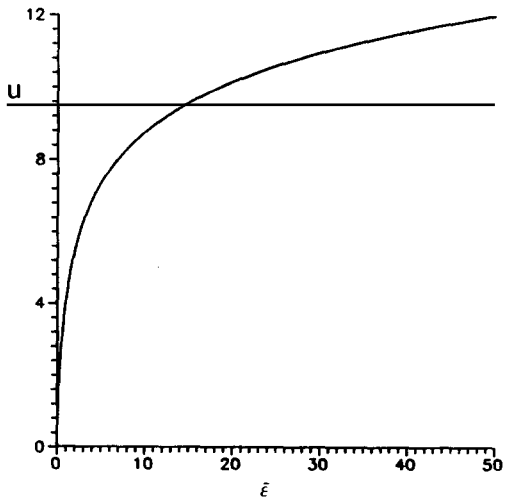

Fig. 17. Stability exponent u of isolated, closed orbit as a function of scaled energy $\tilde{\varepsilon}$.

important for the initial excitation and final recombination process of the closed orbit, which are described by the dipole matrix elements $d^{(-)}_{m=0}(0,0)$ and $d^{(+)}_{m=0}(0,0)$.

Atomic laser excitation from an initial state $|\mathrm{i}\rangle$ by a long and weak laser pulse of constant amplitude $\mathscr{E}$ may be characterized by the time-independent excitation rate

$$\begin{aligned}\Gamma &= -2\,\mathrm{Im}[T_{\mathrm{ii}}(\bar{\varepsilon})]\,|\mathscr{E}|^2 \\ &= \Gamma_0 - (2\pi)^2\delta_{m0}\sum_{M=1}^{\infty}\frac{\sqrt{2\varepsilon}}{\sinh(Mu)}\cdot 2\,\mathrm{Im}\{d^{(+)}_m(0,0)\,\mathrm{e}^{\mathrm{i}M[S(\varepsilon)-\pi]}d^{(-)}_m(0,0)|\mathscr{E}|^2\}_{\varepsilon=\bar{\varepsilon}}\,,\end{aligned} \tag{106}$$

with the mean excited energy $\bar{\varepsilon} = \varepsilon_{\mathrm{i}} + \omega \geq 0$ and Γ_0 denoting the excitation rate in the absence of the static electric field. The energy dependence of this excitation rate reflects the interference between contributions of repeated returns of the excited electron to the Coulomb zone along the closed orbit.

The solid curve in fig. 18 shows the dependence of Γ/Γ_0 on the mean excited energy $\bar{\varepsilon}$. A sodium atom is excited from an energetically low lying s-state by a long and weak laser pulse, which is polarized parallel to the static electric field. The quantum defect of the excited sodium p-states is given by $\alpha = 0.854$. The corresponding hydrogenic result is shown by the dashed curve in fig. 18. Close to threshold, i.e. for $\bar{\varepsilon} \sim 0$, the isolated periodic orbit is almost stable (see fig. 17) and the contributions of many repeated returns significantly contribute to the classical path representation of eq. (106). This gives rise to a characteristic asymmetric lineshape. With increasing energy the isolated orbit becomes more and more unstable. For these energies, the dominant contribution to the excitation rate comes from the term with $M = 1$ of eq. (106), which describes the contribution of the first return of the excited electron to the reaction zone, and the lineshape becomes approximately sinusoidal.

The time dependence of the electronic dynamics may be studied with a radial electronic wave packet which is generated by a short laser pulse. The repeated returns of this wave packet to the reaction zone may be probed, for example, by a second short laser pulse, which induces a transition to some low lying bound state after a time delay Δt. Figure 19 shows the corresponding Raman transition probability as

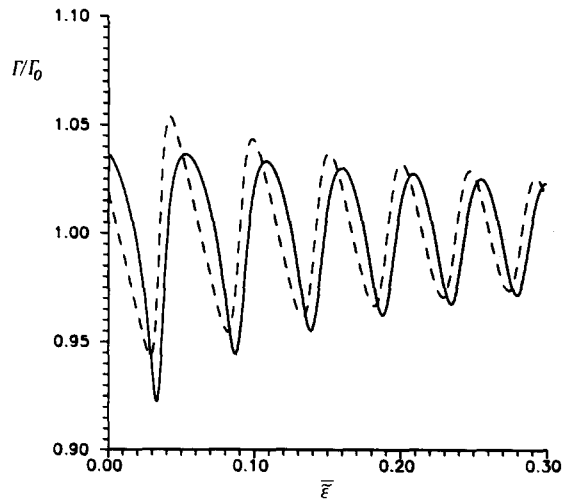

Fig. 18. One-photon excitation rate of sodium (solid curve) and hydrogen (dashed curve) as a function of the mean scaled energy $\bar{\varepsilon}$, for $F = 5.14 \times 10^5\ \mathrm{V\,m^{-1}}$.

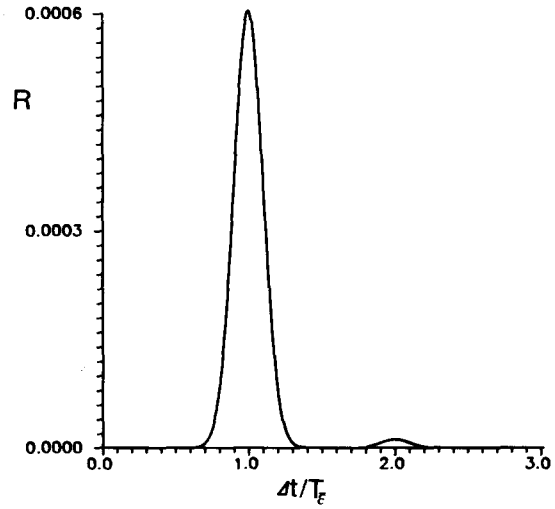

Fig. 19. Two-photon Raman transition probability R as a function of the time delay between both laser pulses, in units of the mean classical orbit time $T_{\bar{\varepsilon}} = 1.7$ ps, for $\bar{\varepsilon} = \varepsilon_{\mathrm{i}} + \omega_{\mathrm{a}} = \varepsilon_{\mathrm{f}} + \omega_{\mathrm{b}} = 5 \times 10^{-4}$ au.

obtained from eqs. (105) and (37) for an electric field strength of $F = 5.14 \times 10^5\ \mathrm{V\,m^{-1}}$. Both laser pulses are assumed to have Gaussian pulse profiles with pulse duration $\tau_p = 0.17\,\mathrm{ps}$. The form of the recombination peaks, which appear at multiples of the classical orbit time, are determined by the pulse profile of the laser pulses, whereas the positions of the maxima and their amplitudes reflect the classical properties of the isolated periodic orbit.

4.3.2. Static magnetic field

In a static magnetic field, $\boldsymbol{B} = B\boldsymbol{e}_z$, the dynamics of a highly excited Rydberg electron is strongly modified at distances $r \geq a = (B/2)^{-2/3}$, at which the diamagnetic interaction potential $V_{\mathrm{ext}}(\boldsymbol{x}) = \frac{1}{8}B^2(x^2 + y^2)$ becomes comparable to the Coulomb potential of the ionic core [4, 103, 146–152]. (The atomic unit of magnetic field strength is given by $B_0 = 2.35 \times 10^5\,\mathrm{T}$.) For magnetic fields of the order of a few Tesla or less the classically accessible region of configuration space is therefore large. This implies large classical actions and laser excitation of Rydberg states in the presence of a weak static, magnetic field may be described with the semiclassical methods of subsection 3.1.2. In particular, atomic transition amplitudes may be expressed as a sum of contributions of all closed orbits of the excited electron which start from the nucleus [36, 99, 100].

The dynamics of a highly excited Rydberg electron in the presence of a Coulomb field and a static magnetic field is particularly interesting, because the corresponding classical Hamiltonian is not integrable and the classical motion exhibits chaos [152]. The axial symmetry of this Hamiltonian around the magnetic field axis implies that closed orbits, which start from the nucleus, are not isolated but form one-parameter families of trajectories. One of these families is shown in fig. 20. Taking into account that contributions from closed orbits within one of these families add constructively, we obtain from eqs. (81), (77) and (65) the classical path representation of the two-photon transition amplitude [36, 100]

$$T_{\mathrm{fi}}(\varepsilon) = T_{\mathrm{fi}}^{(\mathrm{s})} + (2\pi)^{5/2}\mathrm{i}\sum_m \sum_{jM_j} d_m^{(+)}(\theta_j, 0)\sqrt{\sin\theta_j \sin\theta_{0j}}\left|\frac{\partial p_\theta}{\partial\theta_0}\,\frac{\sinh(M_j u_j)}{\sinh u_j}\right|^{-1/2}$$
$$\times\, \mathrm{e}^{\mathrm{i}\{M_j[S_j(\epsilon_m) - m\pi\mu_j^z - \mu_j\pi/2] - \pi/4\}} d_m^{(-)}(\theta_{0j}, 0)\,. \tag{107}$$

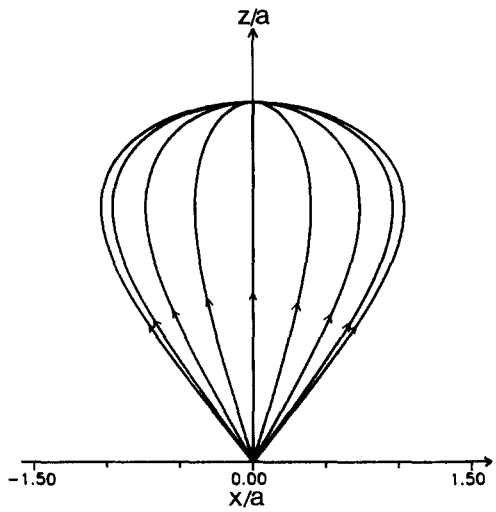

Fig. 20. Schematic representation of the one-parameter family of closed orbits which is denoted by I_2 in table 1.

The energy $\varepsilon_m = \varepsilon + mB/2$ takes into account the threshold shifts due to the paramagnetic interaction term. The index j indicates the different isolated one-parameter families of closed trajectories, which are assumed to be unstable. The quantity μ_j^z denotes their number of crossings of the z-axis. The stability exponents of these orbits are denoted u_j. Table 1 summarizes the classical properties of 14 families of closed orbits for $\varepsilon_m = 0$. In the Coulomb and asymptotic zone, the dynamics of the excited Rydberg electron is invariant with respect to reflection at a plane which goes through the nucleus and is perpendicular to the direction of the magnetic field. Therefore, for each family of orbits of table 1 (except for I_1) there exists also a corresponding family with emission angle $180° - \theta_0$. As the contributions of all closed orbits within one family interfere constructively, their contribution to the two-photon transition amplitude is of order $\lambda^{-1/2}$ instead of $(\lambda^{-1/2})^2$ with $\lambda = \sqrt{a}$ indicating the magnitude of the corresponding classical action.

With the help of a radial electronic wave packet, which is generated by a short laser pulse, we may study the time evolution of an excited electron. As the wave packet leaves the Coulomb zone it is broken up under the influence of the static magnetic field and different parts of it return again to the reaction zone at different times by propagating along one of the isolated families of closed orbits. This wave packet may be probed inside the reaction zone, for example with a second short laser pulse, which induces a transition to some energetically low lying bound state. The corresponding two-photon Raman transition probability is determined by the classical properties of the electronic motion in the neighborhood of these closed orbits.

Figure 21 shows the two-photon Raman transition probability in units of $(\Gamma_0 \tau_p)^2$ as obtained from eqs. (107) and (37) [36] (Γ_0 is the zero-field excitation rate). A sodium atom is excited by a short laser pulse from an initial s-state to Rydberg and continuum states close to the zero-field photoionization threshold and is probed with a second short laser pulse after a time delay Δt. Both laser pulses have identical Gaussian pulse forms with pulse durations $\tau_p = 7.6$ ps and are linearly polarized in the same direction. Figures 21a–c correspond to different angles Θ_{pol} between the static magnetic field and the laser polarization. The magnetic field strength is $B = 0.47$ T. The pulse durations are less than the orbit time of the fastest closed orbits which belong to family I_1. The recombination peaks in figs. 21a–c correspond to repeated returns of various fractions of the generated wave packet to the reaction zone, where they are probed by the second short laser pulse by inducing a transition of the initially prepared

Table 1
Emission and return angles θ_0 and θ, classical action S, orbit time T, $\partial p_\theta/\partial\theta_0$, stability exponent u, Maslov index μ and number of crossings of symmetry axis μ^z of 14 families of closed orbits, which start at the nucleus

orbit	θ_0	θ	$S \times (B/2)^{1/3}$	$T \times (B/2)$	$\frac{\partial p_\theta}{\partial \theta_0} \times (B/2)^{1/3}$	u	μ	μ^z
I_1	90.0	90.0	5.782	2.094	2.816	1.317	3	0
I_2	53.832	53.832	8.580	4.935	10.969	2.892	5	1
I_3	42.810	42.810	10.213	8.111	24.360	3.743	7	2
I_4	37.311	37.311	11.428	11.288	39.272	4.239	9	3
IIb_0	63.649	116.351	12.537	6.739	31.637	3.897	7	2
IIa_1	81.677	128.246	14.233	7.427	56.826	4.291	8	1
IIa_1	51.754	98.323	14.233	7.427	56.826	4.291	8	1
IIb_1	46.679	112.505	14.513	9.568	67.944	4.756	9	3
IIb_1	67.495	133.321	14.513	9.568	67.944	4.756	9	3
IIa_2	79.114	138.459	15.777	10.878	107.925	4.937	10	2
IIa_2	41.541	100.886	15.777	10.878	107.925	4.937	10	2
IIb_2	39.602	110.506	15.884	12.521	97.671	5.144	11	4
IIb_2	69.494	140.398	15.884	12.521	97.671	5.144	11	4
III_1	60.270	60.270	16.158	9.066	108.283	5.144	9	3

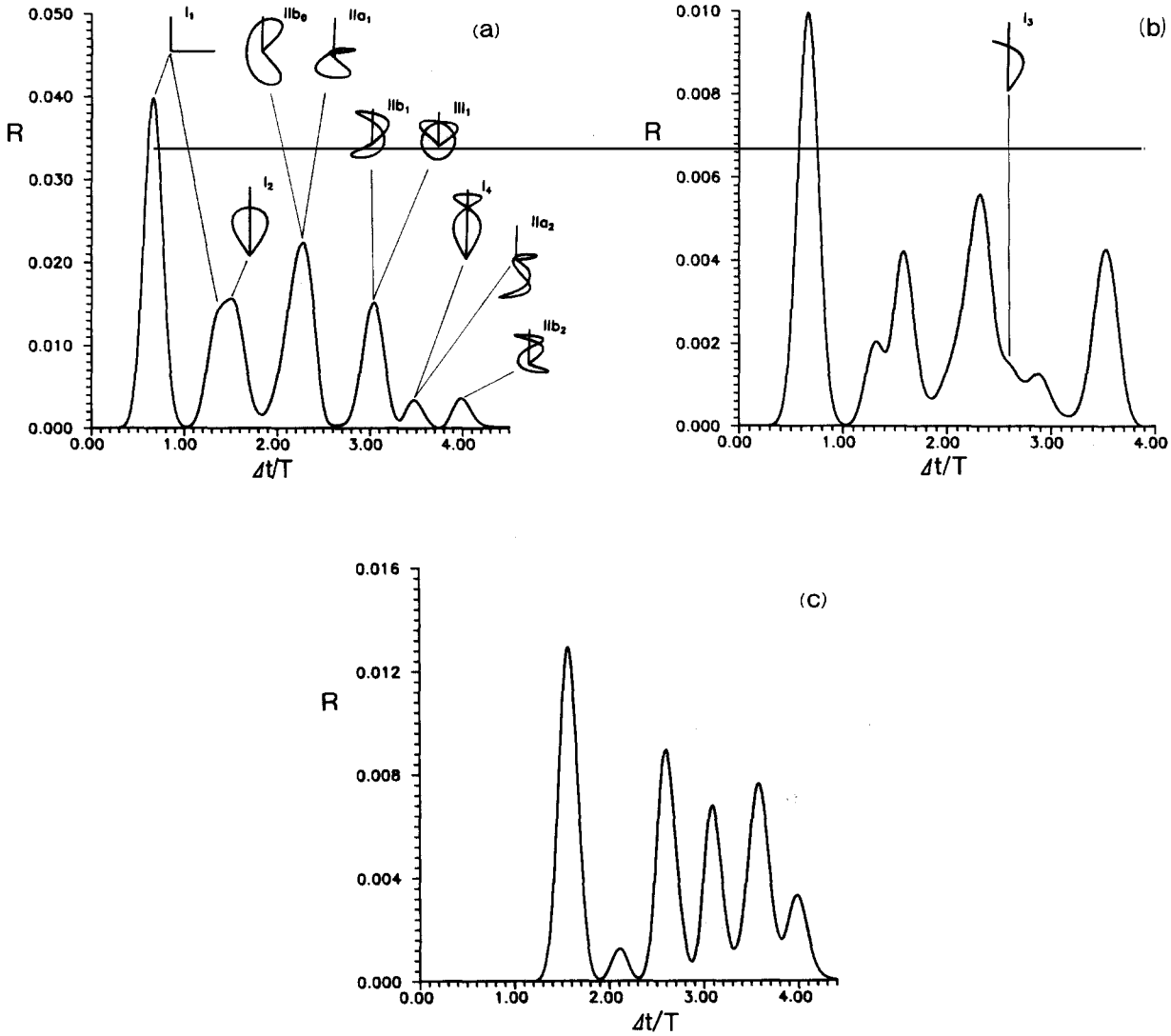

Fig. 21. Raman transition probability R as a function of the time delay between both laser pulses in units of $T = 2\pi/B = 76$ ps ($B = 0.47$ T) with (a) $\Theta_{pol} = 90°$, (b) $\Theta_{pol} = 45°$, (c) $\Theta_{pol} = 0°$.

s-state. On top of each recombination peak the form of one of the closed orbits of the corresponding family is indicated. The vertical straight line indicates the direction of the magnetic field. In fig. 21c the laser polarization is parallel to the magnetic field direction and the angular distribution of the generated wave packet is concentrated around the magnetic field direction. As there is no electron emission perpendicular to the magnetic field, the contribution of orbits I_1 is missing.*)

*) The Raman transition probabilities of figs. 21a,b differ slightly from the corresponding figures of ref. [36]. This difference originates from the dependence of the classical actions $S_j(\varepsilon_m)$ of eq. (107) on the magnetic quantum numbers m, which is due to the paramagnetic interaction term. This m dependence has been neglected in the figures of ref. [36] but is taken into account in figs. 21.

5. Conclusions and outlook

In this review we have summarized work on laser excitation of electronic Rydberg wave packets. These wave packets represent nonstationary, localized electronic states of an atom or molecule which evolve in the Coulomb field of the positively charged ionic core and, possibly, in external fields. Recently, basic features of radial and angular wave packet dynamics have been observed in first experiments, in agreement with theoretical predictions. What remains to be done, and what seems to be the ultimate goal of wave packet generation in Coulomb systems, is the generation of a minimum-uncertainty wave packet moving on a Kepler ellipse which comes closest to a "classical atom". Another interesting perspective is the destruction of coherence of wave packets (for example, their ability to interfere) due to the coupling to (external) fluctuations [153–155]. Finally, we believe that experiments on wave packet dynamics in external fields should be performed, in particular in systems which are not integrable on the classical level. This is a possibility to investigate quantum manifestations of classical chaos.

Acknowledgments

G.A. acknowledges support by the Sonderforschungsbereich SFB 276 "Korrelierte Dynamik hochangeregter atomarer und molekularer Systeme" of the Deutsche Forschungsgemeinschaft. P.Z. was supported by the Österreichische Fonds zur Förderung der wissenschaftlichen Forschung under grant P6008P.

References

[1] A.D. Bandrauk, ed., Atomic and Molecular Processes with Short Intense Laser Pulses (Plenum, New York, 1988).
[2] J.A.C. Gallas, G. Leuchs, H. Walther and H. Figger, Adv. At. Mol. Phys. 20 (1985) 413.
[3] L.F. Mollenauer and J.C. White, eds, Tunable Lasers, Topics in Applied Physics, vol. 59 (Springer, Berlin, 1987).
[4] R.F. Stebbings and F.B. Dunning, eds, Rydberg States of Atoms and Molecules (Cambridge Univ. Press, New York, 1983).
[5] S. Haroche and J.M. Raimond, Adv. At. Mol. Phys. 20 (1985) 347.
[6] T.F. Gallagher, Rep. Prog. Phys. 51 (1988) 143.
[7] C. Greene, U. Fano and G. Strinati, Phys. Rev. A 19 (1979) 1485.
[8] C.H. Greene, A.R.P. Rau and U. Fano, Phys. Rev. A 26 (1982) 2441.
[9] M.J. Seaton, Rep. Prog. Phys. 46 (1983) 167.
[10] J. Dubeau and M.J. Seaton, J. Phys. B 17 (1984) 381.
[11] M. Aymar, Phys. Rep. 110 (1984) 163.
[12] R. Bell and M.J. Seaton, J. Phys. B 18 (1985) 1589.
[13] C. Greene and Ch. Jungen, Adv. At. Mol. Phys. 21 (1985) 51.
[14] U. Fano and A.R.P. Rau, Atomic Collisions and Spectra (Academic Press, New York, 1986).
[15] J. Parker and C.R. Stroud Jr, Phys. Rev. Lett. 56 (1986) 716.
[16] J. Parker and C.R. Stroud Jr, Phys. Scr. T12 (1986) 70.
[17] G. Alber, H. Ritsch and P. Zoller, Phys. Rev. A 34 (1986) 1058.
[18] W.A. Henle, H. Ritsch and P. Zoller, Phys. Rev. A 36 (1987) 683.
[19] H.B. van Linden van den Heuvell, H.G. Muller, J.W. Verschuur and A. ten Wolde, J. Phys. B 20 (1987) L517.
[20] L.D. Noordam, A. ten Wolde, H.G. Muller, A. Lagendijk and H.B. van Linden van den Heuvell, J. Phys. B 21 (1988) L533.
[21] A. ten Wolde, L.D. Noordam, A. Lagendijk and H.B. van Linden van den Heuvell, Phys. Rev. Lett. 61 (1988) 2099.
[22] L.D. Noordam, J.W.J. Verschuur, P. Agostini, H.G. Muller, P. Breger, A. Migus and H.B. van Linden van den Heuvell, J. Phys. B. 22 (1989) L57.
[23] I.Sh. Averbukh and N.F. Perelman, Phys. Lett. A 139 (1989) 449.
[24] J.A. Yeazell, Ph.D. Thesis, The Institute of Optics, Univ. of Rochester.

[25] J.A. Yeazell, M. Mallalieu, J. Parker and C.R. Stroud Jr, Phys. Rev. A 40 (1989) 5040.
[26] L.D. Noordam, H.G. Muller, A. ten Wolde and H.B. van Linden van den Heuvell, preprint.
[27] K. Ellinger, H. Gratl and P. Zoller, in: Proc. EGAS Conf. (Uppsala), Phys. Scr., to be published.
[28] A.I. Andryushin, A.E. Kazakov and M.V. Fedorov, Zh. Eksp. Teor. Fiz. 76 (1979) 1907 [Sov. Phys. - JETP 49 (1979) 966].
[29] J. Javanainen, Opt. Commun. 46 (1983) 175.
[30] G. Alber and P. Zoller, Phys. Rev. A 37 (1988) 377.
[31] M.V. Fedorov and A.M. Movsesian, J. Opt. Soc. Am. B 5 (1988) 850.
[32] G. Alber, Th. Haslwanter and P. Zoller, J. Opt. Soc. Am. B 5 (1988) 2439.
[33] J. Grochmalicki and M. Lewenstein, J. Phys. B 21 (1988) 3285.
[34] G. Alber, Phys. Rev. A 40 (1989) 1321.
[35] M.V. Fedorov and A.M. Movsesian, J. Opt. Soc. Am. B 6 (1989) 1504.
[36] G. Alber, Z. Phys. D 14 (1989) 307.
[37] H. Gratl, G. Alber and P. Zoller, J. Phys. B 22 (1989) L547.
[38] F. Ehlotzky, ed., Fundamentals of Laser Interactions II, Lecture Notes in Physics, vol. 339 (Springer, Berlin, 1989).
[39] S.J. Smith and P.L. Knight, eds, Multiphoton processes, Proc. 4th Intern. Conf. on Multiphoton Processes (JILA, Boulder, CO, 1987) (Cambridge Univ. Press, New York, 1988).
[40] W.A. Molander, C.R. Stroud Jr and J.A. Yeazell, J. Phys. B 19 (1986) L461.
[41] J.A. Yeazell and C.R. Stroud Jr, Phys. Rev. A 35 (1987) 2806.
[42] J.A. Yeazell and C.R. Stroud Jr, Phys. Rev. Lett. 60 (1988) 1494.
[43] A. ten Wolde, L.D. Noordam, A. Lagendijk and H.B. van Linden van den Heuvell, Phys. Rev. A 40 (1989) 485.
[44] L.D. Noordam, A. ten Wolde, A. Lagendijk and H.B. van Linden van den Heuvell, Phys. Rev. A 40 (1989) 6999.
[45] J.C. Gay, D. Delande and A. Bommier, Phys. Rev. A 39 (1989) 6587.
[46] R.G. Hulet and D. Kleppner, Phys. Rev. Lett. 51 (1983) 1430.
[47] J. Liang, M. Gross, P. Goy and S. Haroche, Phys. Rev. A 33 (1986) 4437.
[48] J. Hare, M. Gross and P. Goy, Phys. Rev. Lett. 61 (1988) 1938.
[49] L.S. Brown, Am. J. Phys. 41 (1973) 525.
[50] A.M. Perelomov, Usp. Fiz. Nauk 123 (1977) 23 [Sov. Phys. - Usp. 20 (1977) 703].
[51] J. Mostowski, Lett. Math. Phys. 2 (1977) 1.
[52] M.M. Nieto and L.M. Simmons, Phys. Rev. D 20 (1979) 1321.
[53] M.M. Nieto, Phys. Rev. D 22 (1980) 391.
[54] V.P. Gutschick and M.M. Nieto, Phys. Rev. D 22 (1980) 403.
[55] C.C. Gerry, Phys. Rev. A 33 (1986) 6.
[56] M. Nauenberg, Phys. Rev. A 40 (1989) 1133.
[57] D. Delande and J.C. Gay, Europhys. Lett. 5 (1988) 303.
[58] R. Heather and H. Metiu, J. Chem. Phys. 86 (1987) 5009.
[59] M. Dantus, M.J. Rosker and A.H. Zewail, J. Chem. Phys. 87 (1987) 2395.
[60] J.Avarellos and H. Metiu, J. Chem. Phys. 88 (1988) 4957.
[61] T.S. Rose, M.J. Rosker and A.H. Zewail, J. Chem. Phys. 88 (1988) 6672.
[62] M.J. Rosker, T.S. Rose and A.H. Zewail, Chem. Phys. Lett. 146 (1988) 175.
[63] M.J. Rosker, M. Dantus and A.H. Zewail, J. Chem. Phys. 89 (1988) 6113.
[64] M. Dantus, M.J. Rosker and A.H. Zewail, J. Chem. Phys. 89 (1988) 6128.
[65] V. Engel, H. Metiu, R. Almeida, R.A. Marcus and A.H. Zewail, Chem. Phys. Lett. 152 (1988) 1.
[66] R.A. Marcus, Chem. Phys. Lett. 152 (1988) 8.
[67] M.J. Rosker, M. Dantus and A.H. Zewail, Science 241 (1988) 1200.
[68] A.H. Zewail, Science 242 (1988) 1645.
[69] R. Heather and H. Metiu, Chem. Phys. Lett. 157 (1989) 505.
[70] R.M. Bowman, M. Dantus and A.H. Zewail, Chem. Phys. Lett. 156 (1989) 131.
[71] M. Dantus, R.M. Bowman, J.S. Baskin and A.H. Zewail, Chem. Phys. Lett. 159 (1989) 406.
[72] S.E. Choi and J.C. Light, J. Chem. Phys. 90 (1989) 2593.
[73] V. Engel and H. Metiu, J. Chem. Phys. 90 (1989) 6116.
[74] V. Engel and H. Metiu, J. Chem. Phys. 91 (1989) 1596.
[75] L.D. Landau and E.M. Lifshitz, Quantum Mechanics: Nonrelativistic Theory (Pergamon, New York, 1979).
[76] G. Peach, Mon. Not. R. Astron. Soc. 130 (1965) 361.
[77] G. Peach, Mem. R. Astron. Soc. 71 (1967) 13.
[78] A. Giusti and P. Zoller, Phys. Rev. A 36 (1987) 5178.
[79] M.G. Fink and P. Zoller, Phys. Rev. A 39 (1989) 2933.
[80] R.R. Freeman, W.E. Cooke, L.D. van Woerkom and T.J. McIlrath, in: Fundamentals of Laser Interactions II, Lecture Notes in Physics, vol. 339, ed. F. Ehlotzky (Springer, Berlin, 1989).

[81] P.W. Milonni, J.R. Ackerhalt, N.W. Galbraith and Mei-Li Shih, Phys. Rev. A 28 (1983) 32.
[82] V.Yu. Finkelshtein, Zh. Eksp, Teor. Fiz. 88 (1985) 1527 [Sov. Phys. - JETP 61 (1985) 912].
[83] E. Kyrölä and J.H. Eberly, J. Chem. Phys. 82 (1985) 1841.
[84] V. Finkelstein, preprint.
[85] E. Kyrölä, J. Phys. B 19 (1986) 1437.
[86] M. Abramowitz and I. Stegun, Handbook of Mathematical Functions, Natl. Bur. Stand. Appl. Math. Ser. No. 55 (USGPO, Washington, DC, 1964).
[87] H.B. van Linden van den Heuvell and H. Gratl, private communication.
[88] M.C. Gutzwiller, J. Math. Phys. 8 (1967) 1979; 10 (1969) 1004; 11 (1970) 1791; 12 (1971) 343.
[89] M.V. Berry and K.E. Mount, Rep. Prog. Phys. 35 (1972) 315, and references therein.
[90] R. Balian and C. Bloch, Ann. Phys. 85 (1974) 514.
[91] W.H. Miller, Adv. Chem. Phys. 25 (1974) 69; 30 (1976) 77.
[92] M.V. Berry and M. Tabor, Proc. R. Soc. London A 349 (1976) 101.
[93] M.S. Child, Adv. At. Mol. Phys. 14 (1978) 225.
[94] M.S. Child, ed., Semiclassical Methods in Molecular Scattering and Spectroscopy (Reidel, Dordrecht, 1980).
[95] V.P. Maslov and M.V. Fedoriuk, Semiclassical Approximation in Quantum Mechanics (Reidel, Boston, 1981), and references therein.
[96] J.B. Delos, Adv. Chem. Phys. 65 (1986) 161.
[97] E.B. Bogomolny, Physica D 31 (1988) 169.
[98] B. Eckhardt, Phys. Rep. 163 (1988) 205.
[99] M.L. Du and J.B. Delos, Phys. Rev. A 38 (1988) 1896, 1913.
[100] E.B. Bogomolny, Pis'ma Zh. Eksp. Teor. Fiz. 47 (1988) 445 [JETP Lett. 47 (1988) 526]; Zh. Eksp. Teor. Fiz. 96 (1989) 487.
[101] A. Dalgarno and J.T. Lewis, Proc. R. Soc. A 233 (1955) 70.
[102] D.A. Harmin, Phys. Rev. A 24 (1981) 2491; 26 (1982) 2656.
[103] P.F. O'Mahony, in: Fundamental Processes of Atomic Dynamics, eds J.S. Briggs, H. Kleinpoppen and H.O. Lutz (Plenum, New York, 1987) p. 197.
[104] J. Broeckhove, L. Lathouwers and P. van Leuven, eds, Dynamics of Wavepackets in Molecular and Nuclear Physics, Lecture Notes in Physics, vol. 256 (Springer, Berlin, 1985).
[105] E.J. Heller, J. Chem. Phys. 62 (1975) 1544.
[106] E.J. Heller, Chem. Phys. Lett. 34 (1975) 321.
[107] E.J. Heller, J. Chem. Phys. 64 (1976) 63.
[108] E.J. Heller, J. Chem. Phys. 65 (1976) 4979.
[109] E.J. Heller, J. Chem. Phys. 66 (1977) 5777.
[110] E.J. Heller, J. Chem. Phys. 75 (1981) 2923.
[111] M. Davies and E.J. Heller, J. Chem. Phys. 75 (1981) 3916.
[112] R. Heather and H. Metiu, Chem. Phys. Lett. 118 (1985) 558.
[113] D. Huber and E.J. Heller, J. Chem. Phys. 87 (1987) 5302.
[114] N.E. Henriksen and E.J. Heller, Chem. Phys. Lett. 148 (1988) 567.
[115] D. Huber, E.J. Heller and R.G. Littlejohn, J. Chem. Phys. 89 (1988) 2003.
[116] D. Huber and E.J. Heller, J. Chem. Phys. 89 (1988) 4752.
[117] D. Huber, S. Ling, D.G. Imre and E.J. Heller, J. Chem. Phys. 90 (1989) 7317.
[118] E.J. Heller, J. Chem. Phys. 68 (1978) 2066.
[119] S.Y. Lee and E.J. Heller, J. Chem. Phys. 76 (1982) 3035.
[120] E.J. Heller, J. Chem. Phys. 68 (1978) 3891.
[121] K.C. Kulander and E.J. Heller, J. Chem. Phys. 69 (1978) 2439.
[122] S.Y. Lee and E.J. Heller, J. Chem. Phys. 71 (1979) 4777.
[123] R.L. Sundberg and E.J. Heller, Chem. Phys. Lett. 93 (1982) 586.
[124] D.J. Tannor and E.J. Heller, J. Chem. Phys. 77 (1982) 202.
[125] A.B. Myers, R.A. Mathies, D.J. Tannor and E.J. Heller, J. Chem. Phys. 77 (1982) 3857.
[126] G. Drolshagen and E.J. Heller, J. Chem. Phys. 79 (1983) 2072.
[127] G. Drolshagen and E.J. Heller, J. Chem. Phys. 82 (1985) 226.
[128] G. Drolshagen, Comments At. Mol. Phys. 17 (1985) 47.
[129] N.E. Henriksen, Comments At. Mol. Phys. 21 (1988) 153.
[130] F. Penent, D. Delande, F. Biraben and J.C. Gay, Opt. Commun. 49 (1984) 184.
[131] F. Penent, D. Delande and J.C. Gay, Phys. Rev. A 37 (1988) 4707.
[132] R.R. Freeman and N.P. Economu, Phys. Rev. A 20 (1979) 2356.
[133] S. Feneuille, S. Liberman, J. Pinard and A. Taleb, Phys. Rev. Lett. 42 (1979) 1404.
[134] W.L. Glab and M.H. Nayfeh, Phys. Rev. A 31 (1985) 530.
[135] H. Rottke and K.H. Welge, Phys. Rev. A 33 (1986) 301.

[136] A.G. Aronov and A.S. Ioselevich, Zh. Eksp. Teor. Fiz. 74 (1978) 1043 [Sov. Phys. - JETP 47 (1978) 548].
[137] A.R.P. Rau, J. Phys. B 12 (1979) L193.
[138] E. Luc-Koenig and A. Bachelier, J. Phys. B 13 (1980) 1743, 1769.
[139] W.P. Reinhard, J. Phys. B 16 (1983) L635.
[140] D. Farrelly and W.P. Reinhard, J. Phys. B 16 (1983) 2103.
[141] V.D. Kondratovich and V.N. Ostrovsky, J. Phys. B 17 (1984) 1981, 2011.
[142] D.A. Harmin, Comments At. Mol. Phys. 15 (1985) 281.
[143] T.P. Grozdanov, P.S. Krstic, M.J. Rakovic and E.A. Solovev, Phys. Lett. A 132 (1988) 262.
[144] D. Wintgen, J. Phys. B 22 (1989) L5.
[145] G. Alvarez and H.J. Silverstone, Phys. Rev. Lett. 63 (1989) 1364.
[146] W.R.S. Garton and F.S. Tomkins, Astrophys. J. 158 (1968) 839.
[147] A. Holle, G. Wiebusch, J. Main, J. Hager, H. Rottke and K.H. Welge, Phys. Rev. Lett. 56 (1986) 2594.
[148] G.R. Welch, M.M. Kash, C. Iu, L. Hsu and D. Kleppner, Phys. Rev. Lett. 62 (1989) 893, 1975.
[149] C. Iu, G.R. Welch, M.M. Kash, L. Hsu and D. Kleppner, Phys. Rev. Lett. 63 (1989) 1133.
[150] M. Yu. Sumetskii, Zh. Eksp. Teor. Fiz. 83 (1982) 1661; 94 (1988) 87 [Sov. Phys. - JETP 56 (1982) 959; 67 (1988) 49].
[151] P.F. O'Mahony and K.T. Taylor, Phys. Rev. Lett. 57 (1986) 2931.
[152] For a comprehensive list of references of experimental and theoretical work on the problem of hydrogen in a static magnetic field, see H. Friedrich and D. Wintgen, Phys. Rep. 183 (1989) 37.
[153] C.M. Savage and D.F. Walls, Phys. Rev. A 32 (1985) 2316.
[154] A.J. Leggett, S. Chakravarty, A.T. Dorsey and M.P.A. Fisher, Rev. Mod. Phys. 59 (1987) 1; Phys. Rev. A 32 (1985) 2316.
[155] A.S. Parkins, C.W. Gardiner and M.L. Steyn-Ross, preprint.